Spatial variation in exploited metapopulations obscures risk of collapse

Daniel K Okamoto[a,b,c], Margot Hessing-Lewis[b], Jameal F Samhouri[d], Andrew O Shelton[d], Adrian Stier[e], Philip S Levin[f,g], and Anne K Salomon[b,c]

[a]Department of Biological Science, Florida State University, Tallahassee, Florida 32303, USA
[b]Hakai Institute, PO Box 309, Heriot Bay, BC V0P 1H0, Canada
[c]School of Resource and Environmental Management, Simon Fraser University, 8888 University Drive, Burnaby, B.C. V5A 1S6, Canada
[d]Conservation Biology Division, Northwest Fisheries Science Center, National Marine Fisheries Service, National Oceanic and Atmospheric Administration, 2725 Montlake Blvd. East,Seattle, WA 98112, USA
[e]Department of Ecology, Evolution, and Marine Biology, University of California, Santa Barbara, CA 93106, USA
[f]The Nature Conservancy, 74 Wall St, Seattle, WA98121, USA
[g]School of Environment and Forestry Sciences, University of Washington, Seattle, Washington, USA

Corresponding Author
Daniel K Okamoto
Department of Biological Science
The Florida State University
Tallahassee, Florida 32303
Phone: (850) 645-9532
emaildokamoto@bio.fsu.edu

Author contributions
DKO designed, built and conducted analyses. AS conducted the home-range literature review. DKO and AKS wrote the initial manuscript draft. DKO, MHL, JFS, AOS, AS, PSL, and AKS initiated the research focus, refined analyses and contributed to revisions

Abstract

Unanticipated declines among exploited species frequently occur despite harvests that appear sustainable. This is common in the oceans, where spatial scales of management can be mismatched with spatially dynamic metapopulations. We explore causes, consequences and potential solutions for spatial mismatches in metapopulations of an important forage fish by combining empirical analysis, numerical modeling and novel theory. We show that spatial complexity can promote stability at large scales, however ignoring complexity produces cryptic and negative consequences at small scales. Harvesting metapopulations magnifies spatial variability, which creates discrepancies between regional and local trends while increasing risk of local population collapses. Such effects asymmetrically impact locally constrained fishers and predators, which are more exposed to risks of cryptic collapses. Importantly, we show that dynamically optimizing harvest can minimize local risk without sacrificing yield. Thus, multiple nested scales of management can help avoid cryptic collapses and the ensuing ecological, social and economic consequences.

Keywords: Metapopulation, Fisheries, Population Dynamics, Conservation, Natural Resource Management

Introduction

Mismatches in spatial scale create pervasive problems in ecology and natural resource management (1). This occurs in part because the spatial extent of management or conservation units are often defined by history, jurisdictional, or institutional criteria rather than the scale of social and ecological processes at play (1-6). Such choices about the scale of management can result in mismatches, where feedbacks controlling interactions among groups occur at different spatial scales. In managed ecosystems like forestry and fisheries, mismatches may occur when harvest recommendations are based on trends in large-scale abundance without accounting for localized collapses (7). Yet these spatially isolated collapses can have far-reaching consequences when that species plays an indispensable role in local social-ecological systems, including human communities with limited capacity to forage over wide geographic scales. Empirical identification of appropriate spatial scales of management remains difficult for spatially structured populations, but can be a pre-requisite for diagnosing and reconciling challenges that spatial mismatches impose on the sustainable and equitable use of natural resources.

In metapopulations - plant or animal populations connected through dispersal - the dynamics of individual populations can differ substantially from the aggregate metapopulation (3, 4, 8-11). A combination of movement, shared climate drivers, and compensatory processes determine whether dynamics of individual populations reflect the dynamics of the aggregate metapopulation (12). Consideration of metapopulation structure has improved the management of the spotted owl (*Strix occidentalis*) (13), salmon (*Onchorhyncus* spp.) (14-16), amphibians (17), and mosquitoes (18). To date, efforts to integrate metapopulation dynamics into natural resource management have largely focused on either minimizing extirpations (19), characterizing productivity of the metapopulation as a whole (sensu 20), or valuing benefits of portfolio effects (i.e. stabilizing effects of spatial asynchrony sensu 21). Less understood, both in theory and in practice, is how mismatches in spatial scale, governed by the interaction between resource exploitation and metapopulation properties, affect spatial variability, frequency of localized collapses, and their ecological and social consequences across spatial scales.

In this study, we assess how spatial differences in harvest rates interact with animal movement and recruitment to shape patterns of population variability and risk of collapse at different spatial scales. Our results illustrate the challenge in managing spatially complex populations using three complementary approaches. Our empirical case study of a managed stock of Pacific herring (*Clupea pallasii*) in Canada's Pacific coast highlights the discrepancies among scales in both population dynamics and harvest rates. Further, for this system, we use multiscale risk analysis using closed-loop simulation modeling to highlight the impacts of scale mismatch. In doing so we demonstrate the potential value of optimized spatial management in reduction of risk and inequity. We contextualize such spatial risks by conducting a review of herring predator home-range size. Finally, we generalize these results by developing new theory

to evaluate how exploitation of metapopulations can alter spatial and temporal variability at different spatial scales and thus affect spatial inequities in risk exposure.

Empirical Pacific herring case study in British Columbia's Central Coast

Pacific herring exemplify the challenges inherent to managing metapopulations. In British Columbia (BC), Canada (Fig 1a), herring return annually to nearshore coastlines in the late winter/early spring to reproduce. During this annual migration, they are harvested and preyed upon by a range of consumers. Mobile commercial fishing fleets harvest adult herring for their roe in the days prior to spawning; in contrast, indigenous fishers, constrained to a local area, harvest both adult herring and their eggs after spawning events as an important food, trade and cultural resource (22-26). Unfortunately, a core uncertainty for herring management, as for many species, is the extent of movement between areas (27-32)**.** Similar uncertainty surrounds spatial variation in spawning biomass (i.e. 33), which may result in part from the degree of demographic synchrony between areas (e.g.. synchrony in recruitment). Pacific herring in British Columbia are currently managed as stocks at regional (100s of kilometers) scales by Canada's federal fisheries agency. Within these stocks, multiple spawning aggregations (substocks) seasonally occupy individual stretches of coastline, many of which are of important traditional and cultural value to indigenous groups. Thus, Pacific herring fisheries present a valuable system in which to explore how spatial population dynamics, scales of management, and spatial constraints of fishers and predators interact to influence differential risk exposure to population collapses.

Results

Empirical Pacific Herring Case Study: British Columbia's Central Coast

Spatiotemporal variability in Pacific herring biomass and catch

Pacific herring subpopulations on the Central Coast of BC exhibit substantial temporal and spatial variability (Fig 1a, b, c). The estimated biomass of individual ("local") subpopulations has varied by more than an order of magnitude over the past three decades, and similar differences in population size are evident among subpopulations in the same year. As a consequence, aggregate ("regional") stock biomass at any one point in time is bolstered by a few subpopulations, while others linger at low levels (Fig1b, SI Fig S.1). Synchrony in biomass among subpopulations is low (0.29), with much higher variability at the subpopulations scale (avg. CV = 0.88) than in aggregate (CV = 0.54). This discrepancy results from high spatial variability in subpopulations trends [Fig 1c - also known as β variability (34)].

This discrepancy between variability at the metapopulation (stock) and local subpopulation scales challenges the management objective of maintaining a target harvest rate of 20%. In fact as much as an estimated 91% of an individual subpopulation's biomass is harvested annually, though the aggregate exploitation rate fluctuates around the target of 20% (Fig 1d, e, SI Fig S.2)**.** Counterproductively, this can result in occurrences where subpopulations experiencing periods

of lower-than-average biomass are heavily exploited preceding collapse (e.g. Fig 1d, in 2006). Harvest rates generally differ in magnitude among subpopulations in any given year (SI Fig S.2) and higher harvest rarely focus on the subpopulations with highest biomass (SI Fig S.2). This is illustrated directly by uneven spatial harvest distributions (SI Fig S.2), which we measured as the deviations from two baselines of spatial harvest evenness used here and in the simulation model. These are: proportional allocation* or an optimized allocation†. We explore the potential consequences of different spatial harvest distributions via a closed-loop simulation model (see *Spatial risk analysis* section below).

Foraging-ranges of select Pacific herring predators

Consumers that depend on Pacific herring for food vary dramatically in the spatial scales at which they operate. Indigenous fishers are spatially constrained by boat size, fuel costs and political/cultural boundaries (Fig 1a, Table 1, 26, 35). In contrast, the commercial fleet of seine and gillnet fishers are highly mobile and can pursue fish throughout the region. Similarly, non-human predators of herring and herring roe have a diversity of home-ranges and therefore interact with herring at multiple scales (Table 1). Many predators rely on herring when they move inshore around spawning season. Many crustaceans (36, 37), echinoderms (38, 39), rockfishes and lingcod (40-45), harbor seals (46, 47) and some seabirds (48-50) and flatfishes (51), exhibit restricted patterns of movement and are likely to exploit one to several major subpopulations, but generally not the entire spatial distribution of the metapopulation (stock). In contrast, humpback whales (52, 53), orcas (54, 55), some seabirds (56), sea lions (54, 57, 58), fur seals (59), halibut (60-62) and gadiforms (63-65) can, given ranges reported, access the geographic area covered by the stock (Table 1, see SI Appendix D). Thus, herring provide food resources to groups with varying movement constraints. As a result, herring population collapses that range from small-scale subpopulations to metapopulation-wide phenomena may have differential impacts on the diverse predators that depend on this resource.

Spatial risk analysis with simulation models of Pacific herring fisheries

We used numerical simulation of a metapopulation to determine whether and under what conditions exploitation rates that appear sustainable in aggregate can risk collapse of local subpopulations, and by extension, adversely affect predators and the fishers who target them at this scale. The divergence in risk among scales, an effect of the mismatch in spatial scale, is

---

*__proportional allocation__: proportional harvest rates are equal among substocks in a given year.
† __optimized allocation__: proportional harvest rates are higher on substocks with more biomass via the ideal free distribution.

controlled by the magnitude of harvest rates, allocation of harvest in space, annual migration, and spatial recruitment synchrony. Our simulations show that risk of collapse[‡] can be 10 times greater at local subpopulation scales than at aggregate metapopulation scales (Fig 2) for the 20% harvest rule. While it may seem intuitive that relatively modest adult migration would minimize differences in risk to subpopulations and the metapopulation, our results do not support this supposition. Even relatively high migration rates can impose substantial discrepancies in the risk of collapse between subpopulation and metapopulation scales (Fig 2). This principle holds so long as spatial synchrony in recruitment is not exceedingly high (Fig 2 upper portions of heatmaps). For most scenarios, high spatial variability (i.e. from low annual migration among subpopulations or low spatial recruitment synchrony) leads to low apparent risk at the aggregate metapopulation scale, despite high risk of collapse for local subpopulations (Fig 2; risk increases towards the lower left quadrants).

We find that risk to local subpopulations greatly exceeds risk to the aggregate metapopulation with both a simulated 10% and 20% target harvest rate. Under the 20% target harvest risk of collapse at the local scale exceeds 10% even with annual migration among subpopulations approaching 50% (Fig 2 h). When harvest is optimized in space or target harvest rates are reduced to 10%, risks of collapse at local scales are dramatically reduced (Fig 2 d,f,i versus Fig 2 h) and limited to scenarios where migration is ~10-15% and spatial synchrony in recruitment is low. Local scale risks of collapse are even worse under a random (or opportunistic) spatial allocation, but also ameliorated by reductions in harvest (SI Fig S.6). Importantly, a 10% target harvest with optimized spatial allocation never exceeded 10% risk of collapse in our simulations.

The discrepancy in risk of collapse at local subpopulation versus aggregate metapopulation scales is shaped by both overall harvest rates and spatial variance in subpopulation trends. Risk at the subpopulation scale matches that of metapopulation scales when subpopulations exhibit little spatial variance (i.e. when there is high recruitment synchrony or high migration, top vs bottom panels in Fig 2 c-j, SI Fig S.4). In contrast, risk diverges with increases in spatial variance. Spatial variance is shaped not only by spatial recruitment synchrony and migration, but also harvest rates and allocation in space. Fig 3b-c illustrates how different harvest allocations impact spatial variation in trends (Fig 3 d, e). Higher harvest rates increase risk at subpopulation scales in part because of higher depletion at the metapopulation scale (Fig 2 c,e,g,i) and also because harvest can increase spatial variance (Fig 3d, explored more generally below with analytical model) when efforts are allocated proportionally. This result demonstrates how low demographic synchrony creates a portfolio effect at the metapopulation scale but simultaneously

[‡] **risk of collapse**: frequency of years with spawning biomass below 20% of unfished biomass

masks risks of collapse at the subpopulation scale which can be exacerbated with higher harvest rates.

However, spatially optimizing harvest rates in space to match local scale variability lowers the risk of subpopulation and aggregate metapopulation collapse (Fig 2 d vs f and Fig 2 h vs i) with no cost to aggregate catch (SI Fig S.5). These results emerge from simulating spatially optimized fishing effort that leaves underperforming locations unexploited and heavily targets overperforming local subpopulations, in accordance with predictions of ideal free distribution theory. Optimal spatial allocation of harvest rates reduces the effects of harvest intensity on spatial variability (Fig 3d) which is strongly related to local risk of collapse (SI Appendix Fig S.4). Thus, approaches that optimize spatial harvest to account for subpopulation dynamics can minimize the spatially destabilizing effect of harvest as well as disparity in exposure to risk of collapse among spatial scales. The benefits of spatially optimized harvest in terms of risk to subpopulations diminishes as migration and spatial synchrony in recruitment productivity decline to low levels (i.e. approach the lower left quadrant of panels in Fig 2c-h, where populations are nearly autonomous with low connectivity).

Theoretical expectations of adult spatial & temporal variability in a metapopulation

To generalize findings from the Pacific herring example, our analytical model explores metapopulation spatial variation mechanistically, starting with changing adult mortality. We find that spatial variation among subpopulations increases with higher total mortality rates (via harvest or otherwise) (Fig 4a) and decreases with migration and synchrony (SI Appendix C), in line with the numerical simulation model results (Fig 3d). As a result, the metapopulation mean and coefficient of variation are less reflective of its subpopulations (Fig 4b). In biological terms, higher mortality decreases mean adult longevity (66) and thereby elevates sensitivity in population fluctuations to recruitment pulses (67-70). The amplification of fluctuations occurs at a higher rate at local scales than on aggregate. This response decreases spatial coupling and predictability. Reduced longevity of adults (via higher mortality) reduces the abundance of adults in each subpopulation that buffers against local stochasticity through survival and migration.

Mathematically, this result emerges for several related reasons. Increases in mortality (constant across space in this case) reduce local population inertia (predictability, measured as 1st order temporal autocorrelation, thick black line in Fig 4c). This reduction in inertia increases population sensitivity to temporal variation in local subpopulation recruitment (red line in Fig 4c). This sensitivity is illustrated by the primary impulse response (Equation 1), which describes how a recruitment perturbation affects the intrinsic growth rate of each subpopulation (red line in Fig 4c). In this case, the response always increases with total mortality (z).

Eq. 1: (Environmental impulse response): $(1-\delta)/(1+e^{-z}+e^{-2z})$

Such increases in local environmental sensitivity reduce spatial coupling (measured as the spatial correlation, dotted black line in Fig 4c) and thereby increase spatial variability in abundance.

These patterns of asynchrony can persist even in the presence of modest migration rates (Fig 4b), another key mechanism explored in our analytical model. In this simple model, temporal variability of local populations is controlled by the combination of migration (δ), mortality (z) and recruitment synchrony in recruitment productivity (synchrony = $(\rho_R + 1)/2$) (Fig 4b, see SI Appendix for solutions). Spatial variation increases directly with decreases in recruitment correlations (ρ_R) and with increases in recruitment variability. We illustrate this graphically for modest migration rates ($\delta = 0.25$) in Fig 4a. Temporal variability at the local subpopulation scale is highly sensitive to movement— spatial variance of adults approaches zero when the population converges to 100% mixing (i.e. as migration approaches 0.5 for two subpopulations) –while aggregate temporal variability of the metapopulation is not.

As a consequence of these combined properties, the risk of collapse at the metapopulation level can obscure or underestimate local scale conservation risks. As with the empirical data and numerical simulation model, aggregate trends can poorly reflect local trends and can appear more predictable than local scale populations. Both analytical and empirical results demonstrate that differences between individual subpopulations and the metapopulation are exacerbated with increases in mortality (due to harvest or otherwise), which increase spatial variation across the metapopulation.

Discussion

Harvest strategies that appear appropriately prescribed at large spatial scales can, at local scales, lead to declines or even effective extirpation of local populations. We call these small-scale declines "cryptic collapses". Specifically, regional harvest strategies can create a "gilded trap" (71) where, in this case, management focuses on the aspects of metapopulations that can benefit conservation and economics at the aggregate scale, but neglect social-ecological inequity in the exposure to risk at local scales. Our results show that spatial mismatch among scales is not merely an esoteric concern. Indeed, they occur in current management situations, and are supported by ecological theory we develop here. Our multiscale risk analysis highlights the impacts of scale mismatch on consumers and the potential value of optimized spatial management for sustainability and equity.

Our work adds critical resolution and understanding to the literature on portfolio effects that is focused on the benefits of spatial variability. Recent work viewing multiple populations as a "portfolio" of assets has shown benefits of maintaining a diversity of populations with high asynchrony. These benefits include reducing local extinctions through so called 'rescue effects' (72-74), providing increased stability in the form of food security for people or animals (75) and minimizing economic risks over large scales by minimizing variance in harvestable abundance

(21). Yet these portfolio analyses typically focus on the attributes of the aggregate metapopulation, whereas the risk of localized population collapse (e.g. depletion below threshold of ecological functionality or socioeconomic value) affects the interests of locally constrained fishers and spatially constrained organisms with small home ranges. Using theory and data we show that the same spatial variation that leads to resilience at the metapopulation scale, when left unaccounted for in management strategies, can also produce unforeseen negative consequences in the form of magnified local risk of collapse.

The consequences of ignoring spatial variation are most severe for spatially constrained communities and predators. In the case of Pacific herring in the Central Coast of British Columbia, local reductions in some subpopulations occurred well before the entire stock showed substantial declines in the mid-2000s. This had greater impact on spatially constrained groups; namely indigenous communities for whom herring is a source of cultural and economic vitality (27, 76, 77), as well as animals with small home ranges that rely on herring. In contrast, mobile fishing fleets and transient predators should be less vulnerable to local depletion events in the short term. Yet in the long term, assumptions of spatial homogeneity can also lead to biased estimates of total productivity (20) that may lead to overly optimistic harvest strategies. Moreover, high local harvest rates may produce sequential depletion over time that eventually erodes the principal of the stock leading to a collapse of the portfolio as a whole.

Pacific herring fisheries on Canada's west coast provide an empirical case where the scale of regional stock assessments masked episodic local overexploitation and subpopulation collapses. Our work exposes inequity among scales in risk exposure, with differentiation among predator groups depending on their home-ranges (i.e. mobile versus non-mobile fishing fleets). Here, high local harvest rates appear to be commonplace even when local subpopulations are depleted (Fig 1) presumably because schooling fish are easy to catch even at low abundances (78). These spatial, scale-dependencies affect which groups or species bear the brunt of management risks, and who reaps the benefits from the portfolio payoff of regional metapopulation stability. Such inequities highlight that ignoring space also excludes critical social, ecological and economic responses central to the triple bottom line (79). While high local harvest rates may have contributed to subsequent local collapses observed in this case study, quantifying other confounding demographics (i.e. spatial variation in stochastic adult mortality) are necessary to explicitly test this hypothesis. While recent local collapses may have occurred in the absence of fishing, fishing is very likely imposing higher population sensitivity to any environmental or biotic influence on recruitment or survival by reducing adult longevity thereby eroding an important buffer against recruitment volatility (80) that we show can contribute to spatial variation.

Importantly, spatial variation in population dynamics is not independent of harvest dynamics. Rather, we demonstrate numerically and analytically that spatial variation is likely to increase with harvest. However, if the distribution of harvest in space can be optimized, we show how the

overall portfolio benefits at multiple scales. Here, demographic asynchrony (in this case asynchrony in recruitment productivity), can be maintained while minimizing subpopulation risk. Translated into practice, our simulation and analytical results highlight two non-mutually exclusive potential solutions for equitably spreading risk among scales: 1) reductions in overall harvest rates can ameliorate biases in risk among scales by reducing baseline levels of risk and reducing effects of harvest on spatial variability. 2) spatially optimizing harvest allocation can minimize spatial variance and ease pressure on at-risk subpopulations, thereby reducing risk of local scale depletion without sacrificing catch. The former creates a trade-off between commercial yield and local risk; the latter between the cost of management and local risk.

Addressing spatial inequity in risk exposure requires confronting these economic and logistical trade-offs. For species such as Pacific herring that have volatile spatiotemporal dynamics and complex migratory phenology (32), polycentric governance structures where governing authorities are nested at different spatial scales may help balance these trade-offs by addressing the problems of fit between ecosystems, social systems and management agencies (26, 81-85). Such systems can capitalize on scale-specific ecological knowledge (including local, traditional and scientific knowledge), scientific capacity and socioeconomic experience to 1) guide decision analyses, 2) co-coordinate data collection and harvest allocation in space, and 3) test policies [e.g. in the Maine Lobster fishery (86)]. Polycentric management schemes are not a silver bullet. However, for systems like Pacific herring where placed-based indigenous fishing communities often object to purely centralized scales of management for social, ecological and economic reasons (26, 27, 76, 77, 87), opportunities to integrate knowledge and objectives into management strategies (and their evaluation) at smaller spatial scales is well placed in managing these fisheries, and may be critical to their perpetuity.

The models used to generate inference in this study are simple in comparison to the nature of complex stochastic systems in space. We ignore many scenarios that are likely to further complicate spatial patterns (i.e. behaviorally or geographically complex migration, spatial and age specific mortality, spatially complex density dependence, Allee effects, cost and data limitations for spatial management, etc.). However, the principles from our simulation and analytical models should generalize regardless of the degree of complexity in the system: a precautionary approach cognizant of resource users across multiple spatial scales may necessitate the incorporation of some degree of locally based management to minimize spatial discrepancies in risk exposure. Overall, our models suggest a mixture of management scales may be key to selecting and implementing harvest levels, and informing how regional harvest is coordinated in space to navigate towards both sustainable and equitable outcomes (83).

Our analyses illustrate the importance of considering spatial dynamics for determining how to most effectively balance equity in management and conservation strategies aimed at achieving social, economic and ecological outcomes (88, 89). These issues are often ignored by centralized management and conservation initiatives focused on larger spatial scales. For over half a

century, fisheries scientists have debated how best to exploit and conserve "mixed stocks" that have separate dynamics but are inseparable in space with the aim of balancing conservation of weak stocks and maximizing total yields (90). Our work inverts this focus to metapopulations, populations with inseparable dynamics that are separated in space. We show how, in these settings, exploitation can magnify local scale fluctuations and spatial variability. As a result aggregate metrics poorly represent local scale dynamics (Fig 3d,e, Fig 4) and the risk of collapse at the local scale increases at a greater rate than the aggregate large scale (Fig 2). This phenomenon creates cryptic collapses with ensuing discrepancies in risk exposure. Fortunately, the magnitude of these discrepancies can potentially be controlled by lowering harvest rates or seeking harvest dynamics that are spatially optimized (Fig 3). Overall, these conclusions are relevant not only to Pacific herring fisheries, but also to the great number of exploited resources that exhibit spatial structure and are valuable to species and people that operate on multiple scales.

Methods

Empirical Pacific Herring Case Study in the British Columbia's Central Coast

Foraging-ranges of select Pacific herring predators

References were searched for using a combination of Web of Science and Google Scholar. Searches were conducted for papers published before April 2017 using various combinations of the following terms: The scientific and common name of target species, range, foraging range, home range, migration, telemetry, tracking, and movement. Range sizes were determined based on results directly reported in the text of each study, or derived from data included in supplementary materials.

Spatiotemporal variability in Pacific herring biomass and catch

To estimate patterns of spatial and temporal variability in herring biomass and harvest rates, we used spawn deposition and harvest data for six major Pacific Herring spawning units (groupings of spawn sections) that comprise the Central Coast stock in British Columbia, Canada. In the Central Coast, sections are delineated by spatially isolated spawning aggregations. The remaining sections comprised less than 1% of the biomass across the time series duration. Briefly, SCUBA surveys are used to estimate herring egg abundance which is converted to total spawning biomass with the assumed conversion of ~100 eggs/g and an equal sex ratio (25, 91). Catch (which occurs in the days prior to spawning) is reported by geographic section. For full description of the time series see (25) and references therein.

To reconstruct spatial biomass from the biomass and harvest time series observations, we use a nonlinear model in a Bayesian hierarchical state-space framework. We modeled biomass as:

Eq. 2: $\hat{b}^{+}_{t+1,l} = \exp\left[\alpha_l + (1-\beta_l)\ln\left[b_{t-1,l}\right] + \lambda_l b_{t,l}\right.$

where, $\hat{b}^{+}_{t+1,l}$ is the expected pre-spawn biomass at site *l* in year *t*+1 given the estimate of spawning biomass after harvest from previous years ($b_{t,l}$), growth parameters of a Gompertz model (α_l & β_l) and a survivorship term (λ_l). We estimate latent spawning biomass following harvest ($b_{t,l}$) and convert to pre-harvest biomass by adding known local harvest ($h_{t,l}$).

The latent biomass vector $\boldsymbol{b}_t = [b_{1,t}\ b_{2,t} \ldots b_{L,t}]'$ has a multivariate normal conditional probability:

Eq. 3: $\ln[\boldsymbol{b}_t + \boldsymbol{h}_t] \sim \mathrm{MVN}(\ln \hat{\boldsymbol{b}}^{+}_t, \boldsymbol{\sigma}\Omega)$

We adjust the log-probability for the change of variables by the log-Jacobian of the transformed left-hand side of the equation (92). Ω is the process error correlation matrix and $\boldsymbol{\sigma}$ is the vector of within-site process standard deviations.

We assume the observed spawning biomass ($\mathrm{obs}[b_{t,l}]$) is lognormally distributed:

Eq. 4: $\mathrm{obs}[b_{t,l}] \sim \mathrm{lognormal}(\ln b_{t,l} + \ln q, \sigma_{obs})$

where ln q is the log-proportion of spawning biomass that is observable, with a normal prior borrowed from the herring assessment (25). The lognormal observation error (σ_{obs}) has a half-Cauchy prior with scale parameter 2.5.

We modeled the location specific parameter vectors in a multivariate, hierarchical framework as:

Eq. 5: $\Theta_l \sim \mathrm{MVN}(\Theta_\mu, \boldsymbol{\sigma}_\Theta \Omega_\Theta)$

Where $\Theta_l = [\alpha_l \quad \mathrm{logit}(\beta_l) \quad \mathrm{logit}(\lambda_l)]'$. Elements of the mean parameter vector Θ_μ were given a normal prior with mean 0 and sd = 1.5 (which is approximately uniform on the untransformed scale). Ω_Θ is the process error correlation matrix and $\boldsymbol{\sigma}_\Theta$ is the vector of within-site process standard deviations. We used a Lewandowski-Dorota-Joe LKJ prior (93) for the Cholesky decomposition of the correlation matrices (Ω and Ω_Θ) and the vectors of process standard deviations ($\boldsymbol{\sigma}$ and $\boldsymbol{\sigma}_\Theta$). We estimated the models using Stan (92, 94-96) via R (97) with 3, 1000 iteration chains after burn-in.

We used the model posterior to calculate 1) total biomass at each site at each year, 2) metrics of biomass temporal and spatial variation (see SI Appendix A), and 3) the exploitation rate ($h_{t,l}/b_{t,l}$). We compared the observed local harvest rates to the theoretical proportional allocation [sum($h_{t,l}$) /sum($b_{t,l}$)] and optimized allocation of harvest given the quota. The optimized allocation of catch distributes catches in space according to the ideal free distribution. This distribution removes proportionally more biomass from subpopulations with higher biomass and is the spatial allocation of catch that minimizes effort to achieve the overall quota assuming catch per unit effort is linearly related to biomass (see SI Appendix A for mathematical details).

Risk analysis with spatial closed-loop simulation of Pacific herring fisheries

We use a spatial, stochastic model to simulate how spatial metapopulation dynamics and fishing behavior interact to influence risk of overfishing (frequency of years with spawning biomass below 20% of unfished biomass) at the subpopulation and metapopulation scales under a diverse suite of scenarios that include a factorial gradient of 1) annual movement (see Annual adult migration among spawning areas below), 2) environmental recruitment synchrony (the degree of correlation in recruitment in space – see Spatiotemporal Recruitment Dynamics below), 3) a range of harvest rates (see Stock Harvest Quota below), and 4) allocation of harvest in space (see Spatial Harvest Prosecution below).

For all analyses, we simulate 10 subpopulations placed equidistant around a hypothetical island of arbitrary size such that oceanographic distance from subpopulation 1 to 2 is the same as 1 to 10. Fish spawning at any site in a given year can move to any other site in the next year, with a probability that declines with distance. Likewise, synchrony in stochastic recruitment among sites decays with distance. Stochasticity in dynamics is included in recruitment (spatial and temporal variation), survival (temporal variation only) and movement probabilities (spatial and temporal variance).

Abundance of fish in location *l* at age *a* in year *t* is represented by $n_{a,l,t}$. The order of operations mathematically is 1) recruitment, 2) survival, 3) movement, 4) roe fishery harvest, and 5) spawning. The abundance is respectively denoted $n^{++}_{a,l,t}$, (after recruitment and survival [for age 2] or survival [for age 2+]), $n^{+}_{a,l,t}$ (after movement) and $n_{a,l,t}$ (after harvest).

Spatiotemporal Recruitment Dynamics

Following the assumptions of the current British Columbia herring assessments (23, 25), recruitment of age 2 individuals at location *l* is a function of eggs produced 2-years prior at location *l* ($\text{eggs}_{l,t}$) and local density dependence. Recruitment of age 2 individuals is characterized by the Beverton-Holt model:

Eq. 6: $n^{++}_{a=2,l,t+2} = \text{eggs}_{l,t} \exp\left[\epsilon_{l,t} - \frac{{\sigma_r}^2}{2}\right] / (\alpha + \beta \text{eggs}_{l,t})$

Where α and β are stock-recruit parameters [595.25 & 1.79×10^{-8} derived from (23)], $\epsilon_{l,t}$ is the error at time *t* at location *l* with standard devation σ_ϵ , $\text{eggs}_{l,t}$ is the product of abundance at age ($n_{a,l,t}$), maturity [m_a = 0.25 (age 2), 0.9 (3), 1 (4+) from (25)] and female fecundity $\text{f}_a = \exp\,[4.69](\text{w}_a)^{1.13}$ where w_a (grams at age) = $4.5\times10^{-3}(27(1 - \exp\,[-0.48 * \text{age}])^{3.127}$ from (25, 98):

Eq. 7: $\text{eggs}_{l,t} = \sum_{a=2}^{10} \text{m}_a \text{f}_a [0.5 n_{a,l,t}]$

We allow recruitment to exhibit both spatial and temporal variability and autocorrelation with a first-order vector autoregressive model [VAR(1)]:

Eq. 8: $\boldsymbol{\epsilon_t} = \phi\boldsymbol{\epsilon_t} + \mathrm{MVN}(0, {\sigma_r}^2[1-\phi^2]\Omega_r)$

ϕ is a 1st order autoregressive term, and $\mathbf{e}_t$ is a multivariate normal error vector with spatial correlation matrix Ω_r. Spatial correlations follow a Gaussian spatial decay with distance (d), controlled by the standard deviation σ_Ω. For each scenario, σ_r is numerically tuned such that net recruitment variability is approximately constant across scenarios [$\sigma_{r.mu}$ = metapopulation level coefficient of variation = 0.8 (23)].

Adult Survival

All adult survival occurs prior to movement into spawning locations, yielding pre-movement, pre-harvest abundance:

Eq. 9: $n^{++}_{a,l,t+1} = \begin{cases} \lambda_t\, n_{a-1,l,t} & 2 < a < 10 \\ \lambda_t\, n_{a-1,l,t} + \lambda_t\, n_{a,l,t} & a = 10 \text{ (plus group)} \end{cases}$

Survival in any given year is constant in space and is randomly drawn from a beta-binomial with mean λ_t = 0.6 with coefficient of variation of 0.2, derived from (25).

Annual Adult Migration Among Spawning Areas

Survivors migrate to new spawning areas to yield a matrix of pre-spawn, pre-harvest matrix of abundance ($\mathbf{N}_t^{+}$) describing abundance at each age given by the matrix product:

Eq. 10: $\mathbf{N}^{+}{}_t = \mathbf{N}^{++}{}_t\, \mathbf{S}_t$

$\mathbf{S}_t$ is a square matrix of linear migration rates. Row elements of $\mathbf{S}_t$ sum to one and are stochastic Dirichlet realizations with shared scale parameter (scale =10) and a mean migration probability controlled by a scaled Cauchy decay given a distance from site *l* to site *i* ($dist_{l\to i}$) and a migration scaling parameter (γ):

Eq. 11: $\mathrm{P}(migration_{l\to i} \mid dist_{l\to i}, \gamma) = \left[\gamma\left(1+\frac{dist_{l\to i}}{\gamma}\right)^2\right]^{-1} / \sum_{j=1}^{L}\left[\gamma\left(1+\frac{dist_{l\to i}}{\gamma}\right)^2\right]^{-1}$

γ is numerically tuned to achieve a desired retention rate for each scenario. For reference regarding stochasticity, if the mean migration rate is 0.2, the coefficient of variation in migration among years with scale =10 is 0.1.

Stock Harvest Quota

We follow the existing harvest control rules of Pacific herring in British Columbia (23, 25). The annual biomass harvest quota for the stock (Q_{t+1}) is designed to achieve a target harvest rate (H_{Target}) and a minimum spawning escapement (25% of B_0 - the average steady state biomass without fishing).

Eq. 12: $Q_{t+1} = \begin{cases} \min(\, H_{\text{Target}}\, B_{Forecast,t}, B_{Forecast,t} - 0.25B_0 \,) & \text{if } B_{Forecast,t} > 0.25B_0 \\ 0 & \text{otherwise} \end{cases}$

For simplicity, forecast biomass made in year *t* ($B_{Forecast,t}$) for year (*t+1*) is the expected biomass assuming deterministic recruitment (i.e. without stochastic variability). In order to avoid evaluating stock assessment model performance (which is out of the scope of this study) we avoid assessments explicitly within the closed loop. Rather, we assume forecasts are unbiased with no observation noise.

Spatial Harvest Prosecution

We use two spatial fleet allocation scenarios to generate the distribution of spatial harvest given the stock quota (Q_t): 1) the fleet prosecutes the fishery in direct proportion to spawning biomass (proportional allocation) or 2) the fleet is allocated according to the ideal free distribution (IFD) that in theory maximizes catch efficiency. Here, realized catch is nonlinearly related to spawning biomass, harvesting more from areas with higher abundance and leaving alone areas with lower abundance. See SI Appendix B for details in generating the IFD and an additional case with a random spatial allocation more similar to the empirical case study. In all cases, fishery selectivity is identical to maturity-at-age.

Given the local harvest ($h_{l,t}$) produced by these scenarios the post-harvest abundance is:

Eq. 13: $n_{a,l,t} = n^{+}_{a,l,t} - m_a n^{+}_{a,l,t} h_{l,t} / \sum_{a=2}^{10} w_a m_a n^{+}_{a,l,t}$

Simulation details

For each simulation, we ran the following simulation algorithm, which: 1) evaluated deterministic equilibria without fishing, 2) initiated stochastic forcing of recruitment from the equilibrium for 12 years, 3) initiated the fishery, and 4) recorded statistics for years 23-52. We ran 100 replicate simulations for each parameter combination, recording a) mean number of years below 20% B_0 at both stock and substock scales (risk of collapse), b) stock and substock level catch, c) stock and substock biomass, d) stock and substock temporal variability (coefficient of variation) in biomass, and e) spatial variation in biomass (difference between squared coefficient of variation at the substock versus stock scale).

Theoretical impact of mortality, migration and synchrony on spatial and temporal variability in stochastic metapopulations

To evaluate how mortality, migration and demographic synchrony interact to impact temporal variability, spatial variability and sensitivity to a single perturbation for local populations and the metapopulation, we use a stochastic metapopulation model with two populations in discrete time. We convert the model to a first order Vector Autoregressive model (VAR(1)) where statistical properties of stochastic forcing in multivariate systems are well described (99) . We explore this simple model for generality across the diversity of species and

management applications discussed above. Using this model we calculate 1) temporal variability (temporal coefficient of variation) of the populations and metapopulation, 2) spatial variability (the differences between the squared temporal coefficient of variation at the populations and metapopulation), 3) the sensitivity to recruitment via an impulse response analysis that measures how a recruitment pulse propagates through the population, 4) the predictability of the populations as measured by the first-order autocorrelation for the populations, and 5) the spatial coupling measured as the spatial autocorrelation in the metapopulation.

We assume that individuals in the population are mature at age 2, adults move among populations by linear diffusion, all adults are identical, and environmental stochasticity only affects survival of recruits (survival to pre-movement age 2 fish).

Mathematically, the simple model is represented as follows. Let $Y_{a,i,t}$ represent the adults of age a at location i in year t and δ is the per capita annual probability of moving among sites and e^{-M} is the survival rate. Then the equations for dynamics in site i are given as follows.

Total reproduction is the sum of adults across all adult age classes.

Eq. 14: $$Y_{0,i,t+1} = 0.5e^{-M}\sum_{a=1}^{n}(1-\delta)Y_{a,i,t} + \delta Y_{a,j,t}\,,\ \ 0 \le \delta \le 0.5$$

The stock recruit function that determines how zygotes translate into one-year-olds is a Gompertz function:

Eq. 15: $Y_{1,i,t+1} = \alpha(Y_{0,i,t})^{1-\beta}\exp\left[\zeta_{i,t}\right]$

Survival and migration are given by:

Eq. 16: $$Y_{a,i,t+1} = \begin{cases} e^{-M}\left[(1-\delta)Y_{a-1,i,t} + \delta Y_{a-1,j,t}\right] & 2 \le \mathrm{a} \le \mathrm{n}-1 \\ e^{-M}\left[(1-\delta)(Y_{a-1,i,t} + Y_{a,i,t}) + \delta(Y_{a-1,j,t} + Y_{a,j,t})\right] & a = \mathrm{n}\ \text{(plus group)} \end{cases}$$

The vector $\boldsymbol{\xi}_t = [\zeta_{1,t}, \zeta_{2,t}]'$ follows a multivariate normal distribution [i.e. a multivariate extension of the model of Bjornstad et al. (70)] with mean zero and variance-covariance matrix $\boldsymbol{\Sigma}_{\xi}$, whose entries are controlled by variance given by σ_R^2 and covariance controlled by the spatial correlation ρ_R. Thus, synchrony among the two populations is regulated by the spatial correlation in environmental noise and the degree of migration between populations (with a maximum migration probability of 0.5 providing a single, fully mixed population).

To evaluate how the nature of variability is shaped by correlation in recruitment stochasticity (controlled by covariance in $\boldsymbol{\xi}_t$) and how migration probability (δ) influences variability at the local and metapopulation scales, we can cast the model in terms of log-scale deviations from the equilibrium. To do so, we vectorize the variables and convert the log-scale model (i.e $x_{a,i,t} = \ln Y_{a,i,t} - \ln Y_{a,i}^*$ where $Y_{a,i}^*$ is the equilibrium) into a VAR(1) model by linearizing about the equilibrium (70, 100). This approach approximates the deterministic dynamics of the nonlinear

model with a Jacobian matrix (**J**) of first order dependencies and an environmental covariance matrix. As a result, the matrix of coefficients (with plus group summed at age *n*) is given by the block matrix comprised of among and within population age transitions:

Eq. 17: $$\mathbf{J} = \begin{bmatrix} J_1 & J_2 \\ J_2 & J_1 \end{bmatrix}$$

defined by within and population dynamics given by:

Eq. 18: $$J_i = \begin{bmatrix} 0 & \frac{D}{1+\sum_{n=1}^{n-1}\lambda^n} & \frac{(D)\lambda}{1+\sum_{n=1}^{n-1}\lambda^n} & \frac{(D)\lambda^2}{1+\sum_{n=1}^{n-1}\lambda^n} & \cdots & \frac{(D)\lambda^{n-2}}{1+\sum_{n=1}^{n-1}\lambda^n} & \frac{(D)\lambda^{n-1}}{1+\sum_{n=1}^{n-1}\lambda^n} \\ 1-\beta & 0 & 0 & 0 & \cdots & 0 & 0 \\ 0 & D & 0 & 0 & \cdots & 0 & 0 \\ 0 & 0 & D & 0 & \cdots & 0 & 0 \\ \vdots & \vdots & \vdots & \vdots & \ddots & 0 & 0 \\ 0 & 0 & 0 & 0 & \cdots & \frac{D}{\lambda+1} & \frac{(D)\lambda}{\lambda+1} \end{bmatrix}$$

Where $D = (1\text{-}\delta)$ if $J_i = J_2$ and δ if $J_i = J_2$.

The resulting VAR(1) model is:

Eq. 19: $\mathrm{x_t} = \mathrm{J}\,\mathrm{x}_{t\text{-}1} + \mathrm{Z}\boldsymbol{\xi_t}$

Eq. 20: $\mathbf{x}_t = [x_{L=1,a=1,t} \quad \cdots \quad x_{1,n,t} \quad x_{2,1,t} \quad \cdots \quad x_{2,n,t}\,]'$

Z is a 2n x L binary matrix that controls which of the entries in $\mathbf{x}_t$ are subject to stochasticity terms.

We use the known statistical properties of a VAR(1) model (99) in tandem with the moments of a multivariate lognormal to derive the coefficient of variation for the population and metapopulation as well as spatial variation in the metapopulation. See SI Appendix C for derivation. Finally, to evaluate how local environmental sensitivity changes with mortality rate we analyze the model using impulse response analysis for a VAR(1) (99). The impulse response function in this case gives the log-scale adult response to a stochastic environmental shock in $\zeta_{1,t}$ (log-scale unit deviation in recruitment) and is interpreted as the annual intrinsic growth rate response to the shock. See SI Appendix C for details.

Data along with R, Stan and Mathematica code used for this study are available for download from GitHub.

Acknowledgements:

DKO was supported by a Strategic Grant from the National Sciences and Engineering Research Council of Canada to Simon Fraser University. PSL thanks the Gordon and Betty Moore Foundation for their support of the Ocean Tipping Points project and the David and Lucille Packard Foundation for their support of the Ocean Modeling Forum. We thank J. Cleary, A. Frid and lab group of A. Rassweiler for input on the manuscript, and S. Cox, L. Dee, L.

Hauser, B. Hunt, S. Miller, I. McKechnie, S. Pau, T. Pitcher, E. Petrou and W. Smith for discussions that improved the research. We also thank the Heiltsuk and Haida First Nations for their partnership in the NSERC Strategic Grant and the Department of Fisheries and Oceans for providing herring spatial data.

References:

1. Cumming G, Cumming DH, Redman C (2006) Scale mismatches in social-ecological systems: causes, consequences, and solutions. *Ecol Soc* 11(1).
2. Levin SA (1992) The problem of pattern and scale in ecology: the Robert H. MacArthur award lecture. *Ecology* 73(6):1943-1967.
3. Chesson P (1996) Matters of scale in the dynamics of populations and communities. *Frontiers of population ecology*, eds Floyd R, Sheppard A, de Barro P (CSIRO, Victoria, Australia), pp 353-368.
4. Chesson P (1998) Spatial scales in the study of reef fishes: a theoretical perspective. *Aust J Ecol* 23(3):209-215.
5. Englund G, Cooper SD (2003) Scale effects and extrapolation in ecological experiments. *Adv Ecol Res* 33:161-213.
6. Wiens JA, Chr N, Van Horne B, Ims RA (1993) Ecological mechanisms and landscape ecology. *Oikos*:369-380.
7. Johnson T, Wilson J, Cleaver C, Vadas R (2012) Social-ecological scale mismatches and the collapse of the sea urchin fishery in Maine, USA. *Ecol Soc* 17(2).
8. Melbourne BA, Chesson P (2006) The scale transition: scaling up population dynamics with field data. *Ecology* 87(6):1478-1488.
9. Melbourne BA, Chesson P (2005) Scaling up population dynamics: integrating theory and data. *Oecologia* 145(2):178-186.
10. Chesson P, Donahue MJ, Melbourne BA, Sears AL (2005) Scale transition theory for understanding mechanisms in metacommunities. *Metacommunities: spatial dynamics and ecological communities*, eds Holyoak M, Leibold M, Holt R (University of Chicago Press), pp 279-306.
11. Mangel M, Levin PS (2005) Regime, phase and paradigm shifts: making community ecology the basic science for fisheries. *Phil Trans Roy Soc B* 360(1453):95-105.
12. Kendall BE, Bjørnstad ON, Bascompte J, Keitt TH, Fagan WF (2000) Dispersal, environmental correlation, and spatial synchrony in population dynamics. *Am Nat* 155(5):628-636.
13. Lande R (1988) Demographic models of the northern spotted owl (Strix occidentalis caurina). *Oecologia* 75(4):601-607.
14. Peterson DA, Hilborn R, Hauser L (2014) Local adaptation limits lifetime reproductive success of dispersers in a wild salmon metapopulation. *Nat Commun* 5.

15. Rieman B, Dunham J (2000) Metapopulations and salmonids: a synthesis of life history patterns and empirical observations. *Ecol Freshwat Fish* 9(1-2):51-64.

16. Schtickzelle N, Quinn TP (2007) A metapopulation perspective for salmon and other anadromous fish. *Fish Fish* 8(4):297-314.

17. Marsh DM, Trenham PC (2001) Metapopulation dynamics and amphibian conservation. *Conserv Biol* 15(1):40-49.

18. Stephenson RL (1999) Stock complexity in fisheries management: a perspective of emerging issues related to population sub-units. *Fish Res* 43(1):247-249.

19. Chadès I*, et al.* (2011) General rules for managing and surveying networks of pests, diseases, and endangered species. *Proc Natl Acad Sci* 108(20):8323-8328.

20. Takashina N, Mougi A (2015) Maximum sustainable yields from a spatially-explicit harvest model. *J Theor Biol* 383:87-92.

21. Schindler DE*, et al.* (2010) Population diversity and the portfolio effect in an exploited species. *Nature* 465(7298):609-612.

22. McKechnie I*, et al.* (2014) Archaeological data provide alternative hypotheses on Pacific herring (*Clupea pallasii*) distribution, abundance, and variability. *Proc Natl Acad Sci* 111(9):E807-E816.

23. Department of Fisheries and Oceans (2015) Stock Assessment and Management Advice for BC Pacific Herring: 2015 Status and 2016 Forecast. . *Can. Sci. Adv. Sec. Res. Doc* 2015/038.

24. Lepofsky D, Caldwell M (2013) Indigenous marine resource management on the Northwest Coast of North America. *Ecol Process* 2(1):1-12.

25. Martell S, Schweigert J, Haist V, Cleary J (2011) Moving towards the sustainable fisheries framework for Pacific herring: data, models, and alternative assumptions; Stock Assessment and Management Advice for the British Columbia Pacific Herring Stocks: 2011 Assessment and 2012 Forecasts. *Can. Sci. Adv. Sec. Res. Doc* 136:163.

26. von der Porten S, Lepofsky D, McGregor D, Silver J (2016) Recommendations for marine herring policy change in Canada: Aligning with Indigenous legal and inherent rights. *Mar Policy* 74:68-76.

27. Powell M (2012) Divided waters: Heiltsuk spatial management of herring fisheries and the politics of native sovereignty. *West Hist Q* 43(4):463-484.

28. Flostrand LA, Schweigert JF, Daniel KS, Cleary JS (2009) Measuring and modelling Pacific herring spawning-site fidelity and dispersal using tag-recovery dispersal curves. *ICES J Mar Sci* 66(8):1754-1761.

29. Hay D, McCarter P, Daniel K (2001) Tagging of Pacific herring *Clupea pallasi* from 1936 1992: a review with comments on homing, geographic fidelity, and straying. *Can J Fish Aquat Sci* 58(7):1356-1370.

30. Levin PS, Francis TB, Taylor NG (2016) Thirty-two essential questions for understanding the social–ecological system of forage fish: the case of Pacific Herring. *Ecosyst Health Sustain* 2(4).

31. Jones R, Rigg C, Pinkerton E (2016) Strategies for assertion of conservation and local management rights: A Haida Gwaii herring story. *Mar Policy*.

32. Benson AJ, Cox SP, Cleary JS (2015) Evaluating the conservation risks of aggregate harvest management in a spatially-structured herring fishery. *Fish Res* 167:101-113.

33. Siple MC, Francis TB (2016) Population diversity in Pacific herring of the Puget Sound, USA. *Oecologia* 180(1):111-125.

34. Wang S, Loreau M (2014) Ecosystem stability in space: α, β and γ variability. *Ecol Lett* 17(8):891-901.

35. Harris DC (2000) Territoriality, aboriginal rights, and the Heiltsuk spawn-on-kelp fishery. *U. Brit. Colum. L. Rev.* 34:195.

36. Hines AH (1982) Coexistence in a kelp forest: size, population dynamics, and resource partitioning in a guild of spider crabs (Brachyura, Majidae). *Ecol Monogr* 52(2):179-198.

37. Stone RP, O'Clair CE (2001) Seasonal movements and distribution of Dungeness crabs Cancer magister in a glacial southeastern Alaska estuary. *Mar Ecol Prog Ser* 214:167-176.

38. Cieciel K, Pyper BJ, Eckert GL (2009) Tag retention and effects of tagging on movement of the giant red sea cucumber Parastichopus californicus. *N Am J Fish Manage* 29(2):288-294.

39. Mattison J, Trent J, Shanks A, Akin T, Pearse J (1976) Movement and feeding activity of red sea urchins (*Strongylocentrotus franciscanus*) adjacent to a kelp forest. *Mar Biol* 39(1):25-30.

40. Beaudreau A, Essington T (2011) Use of pelagic prey subsidies by demersal predators in rocky reefs: insight from movement patterns of lingcod. *Mar Biol* 158(2):471-483.

41. Green KM, Starr RM (2011) Movements of small adult black rockfish: implications for the design of MPAs. *Mar Ecol Prog Ser* 436:219-230.

42. Jorgensen SJ*, et al.* (2006) Limited movement in blue rockfish *Sebastes mystinus*: internal structure of home range. *Mar Ecol Prog Ser* 327:157-170.

43. Mitamura H*, et al.* (2009) Preliminary study on homing, site fidelity, and diel movement of black rockfish *Sebastes inermis* measured by acoustic telemetry. *Fish Sci* 75(5):1133-1140.

44. Tolimieri N, Andrews K, Williams G, Katz S, Levin P (2009) Home range size and patterns of space use by lingcod, copper rockfish and quillback rockfish in relation to diel and tidal cycles. *Mar Ecol Prog Ser* 380:229-243.

45. Freiwald J (2012) Movement of adult temperate reef fishes off the west coast of North America. *Can J Fish Aquat Sci* 69(8):1362-1374.

46. Peterson SH, Lance MM, Jeffries SJ, Acevedo-Gutiérrez A (2012) Long distance movements and disjunct spatial use of harbor seals (*Phoca vitulina*) in the inland waters of the Pacific Northwest. *PloS one* 7(6):e39046.

47. Ward EJ, Levin PS, Lance MM, Jeffries SJ, Acevedo-Gutiérrez A (2012) Integrating diet and movement data to identify hot spots of predation risk and areas of conservation concern for endangered species. *Cons Lett* 5(1):37-47.

48. Lorenz TJ, Raphael MG, Bloxton TD, Cunningham PG (2017) Low breeding propensity and wide-ranging movements by marbled murrelets in Washington. *J Wildl Manage* 81(2):306-321.

49. Peery MZ, Newman SH, Storlazzi CD, Beissinger SR (2009) Meeting reproductive demands in a dynamic upwelling system: foraging strategies of a pursuit-diving seabird, the marbled murrelet. *The Condor* 111(1):120-134.

50. Barbaree BA, Nelson S, Dugger BD (2015) Marine space use by marbled murrelets Brachyramphus marmoratus at a mainland fjord system in southeast Alaska. *Mar Ornithol* 116:173-184.

51. Moser ML, Myers MS, West JE, O'Neill SM, Burke BJ (2013) English sole spawning migration and evidence for feeding site fidelity in Puget Sound, USA, with implications for contaminant exposure. *Northwest Sci* 87(4):317-325.

52. Dalla Rosa L, Secchi E, Maia Y, Zerbini A, Heide-Jørgensen M (2008) Movements of satellite-monitored humpback whales on their feeding ground along the Antarctic Peninsula. *Polar Biol* 31(7):771-781.

53. Kennedy AS, Zerbini AN, Rone BK, Clapham PJ (2014) Individual variation in movements of satellite-tracked humpback whales *Megaptera novaeangliae* in the eastern Aleutian Islands and Bering Sea. *Endanger Species Res* 23(2):187-195.

54. Fearnbach H*, et al.* (2014) Spatial and social connectivity of fish-eating "Resident" killer whales (*Orcinus orca*) in the northern North Pacific. *Mar Biol* 161(2):459-472.

55. Hauser DD, Logsdon MG, Holmes EE, VanBlaricom GR, Osborne RW (2007) Summer distribution patterns of southern resident killer whales *Orcinus orca*: core areas and spatial segregation of social groups. *Mar Ecol Prog Ser* 351:301-310.

56. Pearce JM, Reed JA, Flint PL (2005) Geographic variation in survival and migratory tendency among North American Common Mergansers. *J Field Ornithol* 76(2):109-118.

57. Kuhn CE, Costa DP (2014) Interannual variation in the at-sea behavior of California sea lions (*Zalophus californianus*). *Mar Mamm Sci* 30(4):1297-1319.

58. Merrick RL, Loughlin TR (1997) Foraging behavior of adult female and young-of-the-year Steller sea lions in Alaskan waters. *Can J Zool* 75(5):776-786.

59. Kuhn C, Ream R, Sterling J, Thomason J, Towell R (2014) Spatial segregation and the influence of habitat on the foraging behavior of northern fur seals (Callorhinus ursinus). *Can J Zool* 92(10):861-873.

60. Loher T (2008) Homing and summer feeding site fidelity of Pacific halibut (*Hippoglossus stenolepis*) in the Gulf of Alaska, established using satellite-transmitting archival tags. *Fish Res* 92(1):63-69.

61. Nielsen JK, Hooge PN, Taggart SJ, Seitz AC (2014) Characterizing Pacific halibut movement and habitat in a Marine Protected Area using net squared displacement analysis methods. *Mar Ecol Prog Ser* 517:229-250.

62. Seitz AC, Loher T, Norcross BL, Nielsen JL (2011) Dispersal and behavior of Pacific halibut *Hippoglossus stenolepis* in the Bering Sea and Aleutian Islands region. *Aquat Biol* 12(3):225-239.

63. Hanselman DH, Heifetz J, Echave KB, Dressel SC (2014) Move it or lose it: movement and mortality of sablefish tagged in Alaska. *Can J Fish Aquat Sci* 72(2):238-251.

64. Rand KM, Munro P, Neidetcher SK, Nichol DG (2014) Observations of seasonal movement from a single tag release group of Pacific cod in the eastern Bering Sea. *Mar Coast Fish* 6(1):287-296.

65. Wespestad VG, Thorsen K, Mizroch S (1983) Movement of sablefish, *Anoplopoma fimbria*, in the northeastern Pacific Ocean as determined by tagging experiments (1971-80). *Fish Bull* 81(2):415-420.

66. Barnett LA, Branch TA, Ranasinghe RA, Essington TE (2017) Old-Growth Fishes Become Scarce under Fishing. *Curr Biol* 27(18):2843-2848. e2842.

67. Beddington JR, May RM (1977) Harvesting natural populations in a randomly fluctuating environment. *Science* 197(4302):463-465.

68. Hsieh C*, et al.* (2006) Fishing elevates variability in the abundance of exploited species. *Nature* 443(7113):859-862.

69. Shelton AO, Mangel M (2011) Fluctuations of fish populations and the magnifying effects of fishing. *Proc Natl Acad Sci* 108(17):7075-7080.

70. Bjørnstad ON, Nisbet RM, Fromentin J (2004) Trends and cohort resonant effects in age-structured populations. *J Anim Ecol* 73(6):1157-1167.

71. Steneck R*, et al.* (2011) Creation of a gilded trap by the high economic value of the Maine lobster fishery. *Conserv Biol* 25(5):904-912.

72. Hill MF, Hastings A, Botsford LW (2002) The effects of small dispersal rates on extinction times in structured metapopulation models. *Am Nat* 160(3):389-402.

73. Secor DH, Kerr LA, Cadrin SX (2009) Connectivity effects on productivity, stability, and persistence in a herring metapopulation model. *ICES J Mar Sci* 66(8):1726-1732.

74. Fox JW, Vasseur D, Cotroneo M, Guan L, Simon F (2017) Population extinctions can increase metapopulation persistence. *Nature Ecol Evol* 1(9):1271.

75. Nesbitt HK, Moore JW (2016) Species and population diversity in Pacific salmon fisheries underpin indigenous food security. *J Appl Ecol* 53(5):1489-1499.

76. Brown F, Brown YK (2009) *Staying the course, staying alive: coastal First Nations fundamental truths: biodiversity, stewardship and sustainability* (Biodiversity Bc Victoria).

77. Gavreau A, Lepofsky D, Rutherford M, Reid M (2017) "Everything revolves around the herring": The Heiltsuk-herring relationship through time. *Ecol Soc* 22(2).

78. Mackinson S, Sumaila UR, Pitcher TJ (1997) Bioeconomics and catchability: fish and fishers behaviour during stock collapse. *Fish Res* 31(1):11-17.

79. Elkington J (1994) Towards the sustainable corporation: Win-win-win business strategies for sustainable development. *Calif Manag Rev* 36(2):90-100.

80. Essington TE*, et al.* (2015) Fishing amplifies forage fish population collapses. *Proc Natl Acad Sci* 112(21):6648-6652.

81. Borgström S, Elmqvist T, Angelstam P, Alfsen-Norodom C (2006) Scale mismatches in management of urban landscapes. *Ecol Soc* 11(2).

82. Berkes F (2006) From community-based resource management to complex systems: The scale issue and marine commons. *Ecol Soc* 11(1).

83. Biggs R*, et al.* (2012) Toward Principles for Enhancing the Resilience of Ecosystem Services. *Annu Rev Environ Resour* 37:421-448.

84. Folke C, Pritchard L, Berkes F, Colding J, Svedin U (2007) The problem of fit between ecosystems and institutions: Ten years later. *Ecol Soc* 12(1).

85. Young OR (2002) *The institutional dimensions of environmental change: fit, interplay, and scale* (MIT press).

86. Acheson JM (2003) *Capturing the commons: Devising institutions to manage the maine lobtser industry* (University Press New England, Lebanon, NH).

87. Thornton TF, Kitka H (2015) An indigenous model of a contested Pacific Herring fishery in Sitka, Alaska. *Int J Appl Geospatial Res* 6(1):94-117.

88. Halpern BS*, et al.* (2013) Achieving the triple bottom line in the face of inherent trade-offs among social equity, economic return, and conservation. *Proc Natl Acad Sci* 110(15):6229-6234.

89. Law EA*, et al.* (2017) Equity trade-offs in conservation decision making. *Conserv Biol*.

90. Ricker W (1958) Maximum sustained yields from fluctuating environments and mixed stocks. *Journal of the Fisheries Board of Canada* 15(5):991-1006.

91. Hay D (1985) Reproductive biology of Pacific herring (*Clupea harengus pallasi*). *Can J Fish Aquat Sci* 42(S1):s111-s126.

92. Carpenter B*, et al.* (2016) Stan: A probabilistic programming language. *J Stat Softw* 20.

93. Lewandowski D, Kurowicka D, Joe H (2009) Generating random correlation matrices based on vines and extended onion method. *J Multivar Anal* 100(9):1989-2001.

94. Hoffman MD, Gelman A (2014) The No-U-Turn Sampler: Adaptively Setting Path Lengths in Hamiltonian Monte Carlo. *J Mach Learn Res* 15:1593-1623.

95. Stan Development Team (2016) Stan: A C++ library for probability and sampling. Version 2.12.0.).

96. Stan Development Team (2016) RStan: the R interface to Stan. Version 2.10.1.).

97. R Core Team (2017) R: A language and environment for statistical computing (R Foundation for Statistical Computing, Vienna, Austria).

98. Tanasichuk R, Kristofferson A, Gillman D (1993) Comparison of some life history characteristics of Pacific herring (*Clupea pallasi*) from the Canadian Pacific Ocean and Beaufort Sea. *Can J Fish Aquat Sci* 50(5):964-971.

99. Lütkepohl H (2005) *New introduction to multiple time series analysis* (Springer, Berlin).

100. Nisbet RM, Gurney W (1982) *Modelling fluctuating populations* (Wiley, New York).

Table 1: Home-range categories of different Pacific herring predator groups. Details of sources and home-ranges are provided in the SI Appendix.

Home-Range Category	**Home-Range Description**	**Herring Predator Groups**
Localized	single local substock *(< 10 km radius)*	Indigenous fishers**, Seabirds*, Flatfishes*, Crustaceans*, Urchins, Cucumbers, Reef Fishes, Rockfishes
Centralized	multiple substocks *(~10-40 km-radius)*	Indigenous fishers**, Seabirds*, Flatfishes*, Crustaceans*, Gadiforms*, Salmonids**, Halibut**, Harbor Seals
Transient	full stock or greater	Seine & Gillnet Fishers, Cetaceans, Sea Lions, Seabirds*, Gadiforms*, Salmonids**, Halibut**

*Varies by species, ** Varies by migration phase, location or individual

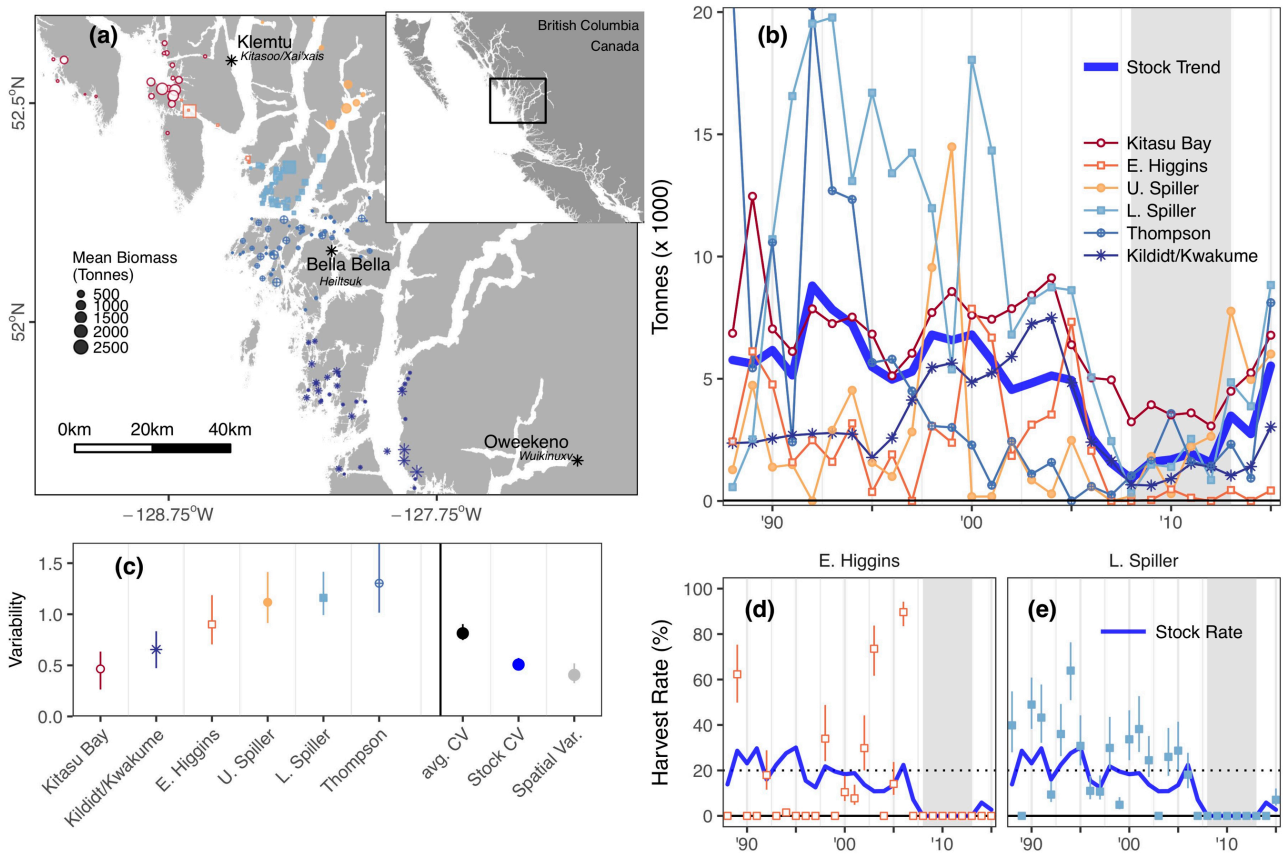

Figure 1: **(a)** Map of major Pacific Herring spawning substocks ("Sections" - denoted by different symbols) as defined by Canada's Federal Fisheries Agency in the Central Coast of British Columbia. Indigenous communities noted with *. **(b)** Estimated trends for the six main substocks (thin colored lines & points) and the metapopulation (stock) mean (thick blue line). Trends were estimated using multivariate hierarchical Bayesian state-space models integrating spawn surveys and catch information. **(c)** Temporal coefficients of variation over 25 years for each substock (points and errorbars), the mean of each substock CV (large black symbol), the regional stock mean (coefficient of variation, blue line), and the spatial variability (black point with error bar) which is the standardized variance of the system after accounting for the variance of the stock and the variance of the substock means. Individual plots for each substock area are shown, along with catch, spawn observations, and 95% posterior credible intervals in SI Appendix A. **(d)** Trends in annual harvest rate for 2 of the 6 local substocks (Higgins and Lower Spiller) with points, 95% credibility intervals and the mean for the aggregate stock (thick blue line). The dotted line represents the target harvest rate of 20%.

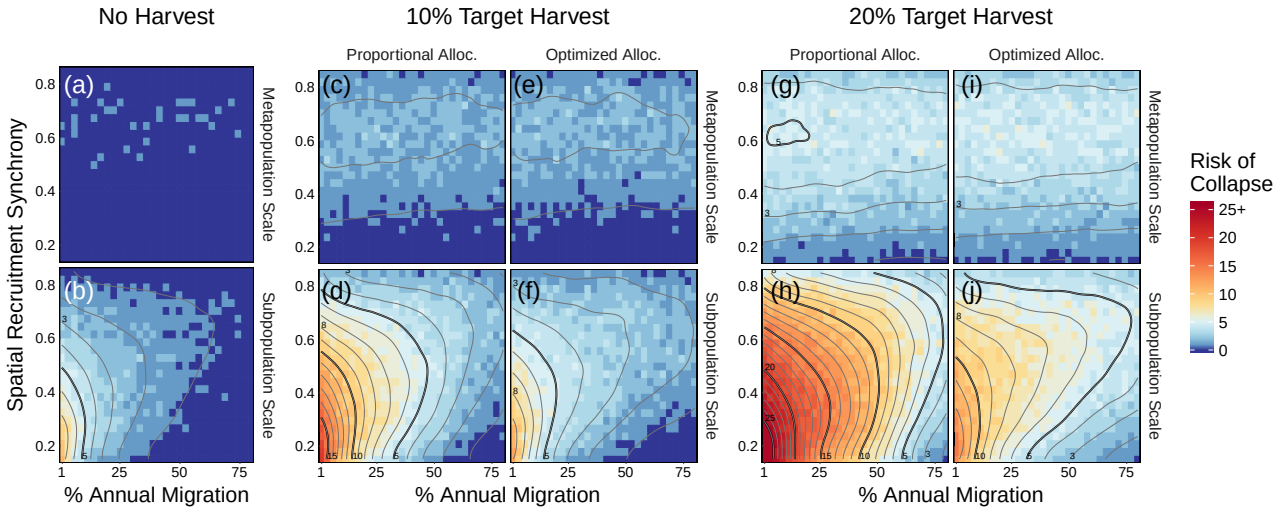

Figure 2: Results of simulation-based risk analysis of hypothetical Pacific herring fisheries under different management and spatial scenarios. Heatmaps show risk of collapse at metapopulation and population scales against annual migration and spatial synchrony in recruitment productivity for different harvest rates and spatial harvest allocation strategies. Risk of collapse is the probability of falling below 20% of unfished equilibrium (i.e. the dotted lines in Fig 3 a-c); at the subpopulation scale, risk is measured as the mean probability of collapse for each population. Optimized spatial allocation removes proportionally less biomass from subpopulations with lower biomass; proportional allocation removes the same proportion of biomass from each subpopulation. Note that differences in mean annual stock level catch among optimized versus proportional allocation are minimal (2c vs. 2e and 2g vs. 2i; SI Appendix B). Annual migration is the mean percent of each subpopulation that emigrates each year. Spatial synchrony in recruitment productivity is $1 + (n-1)\bar{r}$ where $\bar{r}$ is the mean of all unique pairwise correlations in subpopulation recruitment deviations and n is the number of populations. Heatmaps for 30% harvest rules are not shown here as they produce uniformly high risk at both scales. For full results see SI Appendix B.

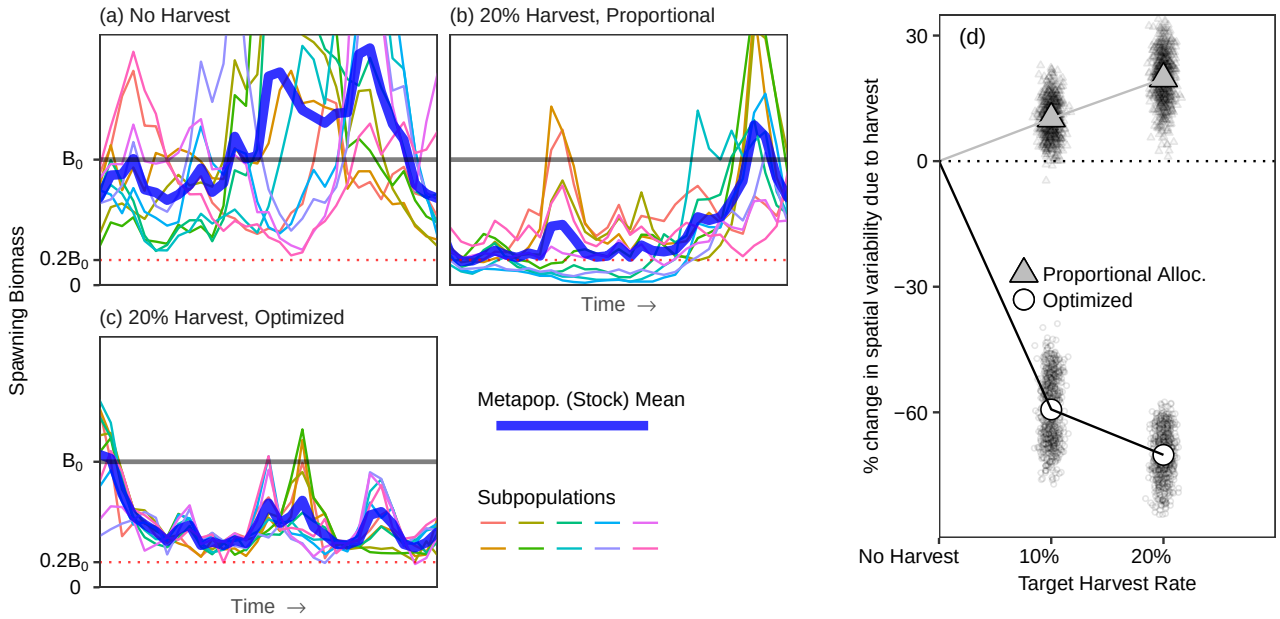

Figure 3: **(a-c)** Example simulations showing spatial variation in biomass measured at the subpopulation level (colored lines) or metapopulation mean (thick blue) for **(a)** an unexploited metapopulation,**(b)** a 20% target harvest allocated proportional to spawning biomass in space, or **(c)** a 20% target harvest allocated optimally in space according to the ideal free distribution. B0 = deterministic biomass in the absence of fishing, dotted line = lower conservation threshold of 20% of B0. **(d)** change in spatial variation for different harvest rates and spatial harvest allocation across different spatial parameter scenarios for migration rates and spatial synchrony. Each point represents the spatial variance from 100 runs from a single 50-year simulation using a unique migration-synchrony parameter combination.

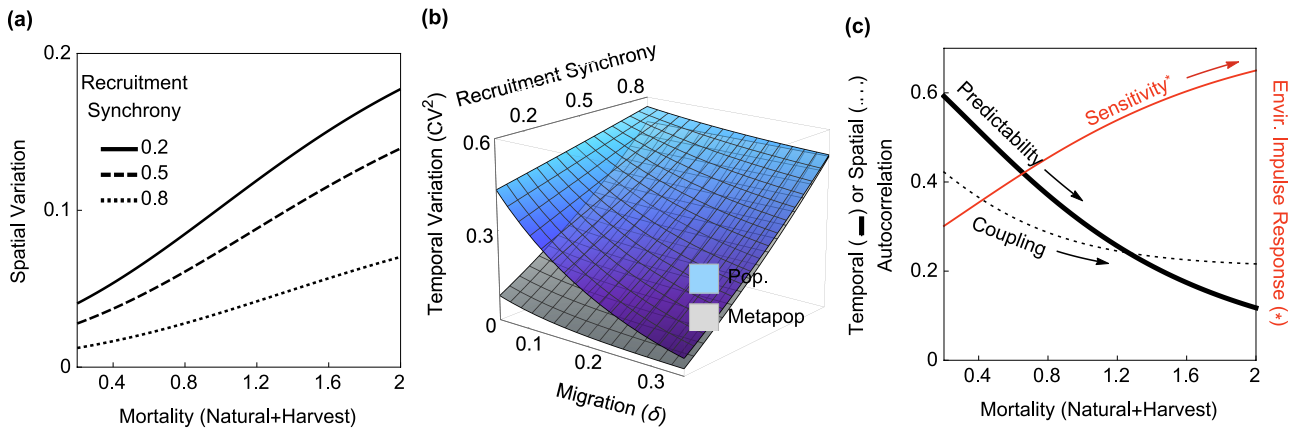

Figure 4: Effect of mortality rate on asynchrony related spatial variability in the metapopulation from the simple two subpopulation model (used for analytical tractability). **(a)** Solutions for spatial variation among populations as a function of total mortality for different levels of spatial synchrony in recruitment productivity when annual migration is 0.25 and log-scale recruitment standard deviation (σ_R) is 0.7 (i.e. CV = 0.8); **(b)** Temporal variability (squared coefficient of variation) of the population and metapopulation. The arrows illustrate spatial variability as the difference between surfaces. **(c)** Measures of local population predictability (measured by first order within population autocorrelation, thick black line), among population coupling (measured by among population correlations, thin black line), and local environmental sensitivity (measured by the response at the population level to a unit environmental impulse affecting recruitment productivity, red line).

Supplementary Information - Appendices for "Spatial variation in exploited metapopulations obscures risk of collapse"

Daniel K Okamoto[a,b,c], Margot Hessing-Lewis[b], Jameal F Samhouri[d], Andrew O Shelton[d], Adrian Stier[e], Philip S Levin[f,g], and Anne K Salomon[b,c]

[a]Department of Biological Science, Florida State University, Tallahassee, Florida 32303, USA
[b]Hakai Institute, PO Box 309, Heriot Bay, BC V0P 1H0, Canada
[c]School of Resource and Environmental Management, Simon Fraser University, 8888 University Drive, Burnaby, B.C. V5A 1S6, Canada
[d]Conservation Biology Division, Northwest Fisheries Science Center, National Marine Fisheries Service, National Oceanic and Atmospheric Administration, 2725 Montlake Blvd. East,Seattle, WA 98112, USA
[e]Department of Ecology, Evolution, and Marine Biology, University of California, Santa Barbara, CA 93106, USA
[f]The Nature Conservancy, 74 Wall St, Seattle, WA98121, USA
[g]School of Environment and Forestry Sciences, University of Washington, Seattle, Washington, USA

Substock trends in Central Coast herring

Residual spatial variability

The residual spatial variation (RSV, also called β variation or the spatial variation due to asynchrony) is the difference between the variance of the mean metapopulation trend and the expected metapopulation mean variance if populations are perfectly correlated. In other words, residual spatial variability is the additional temporal variability at the population level left unexplained by the variability of the metapopulation mean.

While the actual variability of a metapopulation mean given individual variability and covariance of each of N individual population time series (X_i):

$$\mathrm{Var}\left(\frac{1}{N}\sum_{i=1}^{N} X_i\right) = \frac{1}{N^2}\left[\sum_{i=1}^{N}\mathrm{Var}\left(X_i\right) + \sum_{i=1}^{N}\sum_{j\neq 1}^{N-1}\rho_{i,j}\sqrt{\mathrm{Var}\left(X_i\right)\mathrm{Var}\left(X_j\right)}\right] \tag{S.1}$$

$$= \frac{1}{N^2}\left[\sum_{i=1}^{N}\mathrm{Var}\left(X_i\right) + \sum_{i=1}^{N}\sum_{j\neq 1}^{N-1}\mathrm{Cov}\left(X_i, X_j\right)\right] \tag{S.2}$$

$$\tag{S.3}$$

The maximum potential variance of a metapopulation mean given individual variance of each of N populations is:

$$\mathrm{Var}_{\max}\left(\bar{X}\right) = \frac{1}{N^2}\left[\sum_{i=1}^{N}\mathrm{Var}\left(X_i\right) + \sum_{i=1}^{N}\sum_{j\neq 1}^{N-1}\sqrt{\mathrm{Var}\left(X_i\right)\mathrm{Var}\left(X_j\right)}\right] = \left(\sum_{i=1}^{N}\frac{\sqrt{\mathrm{Var}\left(X_i\right)}}{N}\right)^2 \tag{S.4}$$

Hence, the residual spatial variance (RSV) is:

$$\mathrm{RSV}\left(\bar{X}\right) = \mathrm{Var}_{\max}\left(\bar{X}\right) - \mathrm{Var}\left(\bar{X}\right) \tag{S.5}$$

$$= \frac{1}{N^2}\left[\sum_{i=1}^{N}\sum_{j\neq 1}^{N-1}\sqrt{\mathrm{Var}\left(X_i\right)\mathrm{Var}\left(X_j\right)} - \sum_{i=1}^{N}\sum_{j\neq 1}^{N-1}\mathrm{Cov}\left(X_i, X_j\right)\right] \tag{S.6}$$

$$= \frac{1}{N^2}\left[\sum_{i=1}^{N}\sum_{j\neq 1}^{N-1}\left(1-\rho_{i,j}\right)\sqrt{\mathrm{Var}\left(X_i\right)\mathrm{Var}\left(X_j\right)}\right] \tag{S.7}$$

$$= \left(\sum_{i=1}^{N}\frac{\sqrt{\mathrm{Var}\left(X_i\right)}}{N}\right)^2 - \mathrm{Var}\left(\bar{X}\right) \tag{S.8}$$

Similarly, population synchrony as defined by X is given by:

$$\mathit{Synchrony} = \frac{\mathrm{Var}\left(\bar{X}\right)}{\mathrm{Var}\left(\bar{X}\right) + \mathrm{RSV}\left(\bar{X}\right)} \tag{S.9}$$

12 *Full time series results*

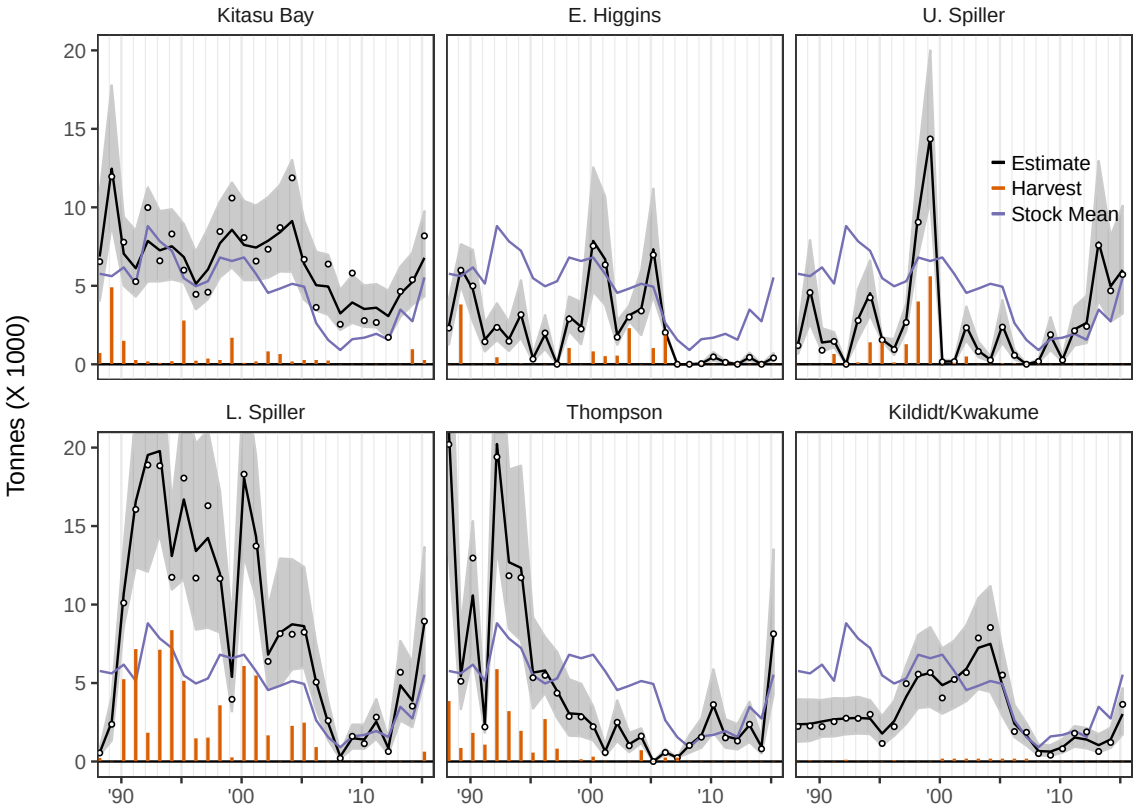

Figure S.1: Trends in pre-spawning biomass (spawn plus catch) and associated catch for the six main spawning locations of Pacific herring the Central Coast of British Columbia. Open points represent the observed pre-spawn biomass, black lines represent posterior estimate of biomass from the model, blue lines represent the overall stock mean, and grey bands are the 95% credible interval of estimated biomass.

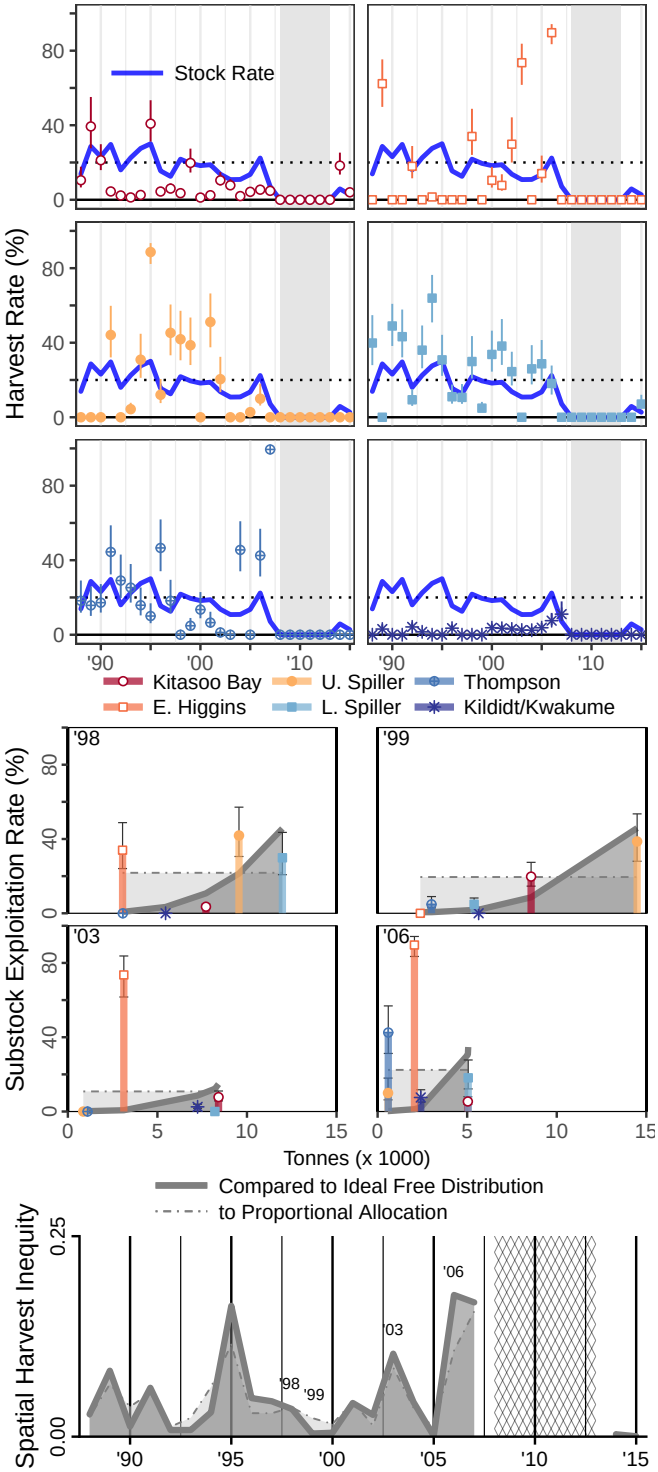

Figure S.2: (a-f) Trends in annual harvest rate for 2 of the 6 local substocks (points and 95% credibility intervals) and the mean for the aggregate stock (thick blue line). The dotted line represents the target harvest rate of 20%. (g-j) Harvest rate and 95% credible intervals for each section in four select years compared to the optimized strategy via the ideal free distribution of harvest (IFD, grey band) or stock allocation with uniform proportional harvest (solid blue line). Points above both the IFD and the equal stock allocation may represent a suboptimal harvest strategy. In contrast, points along the IFD line, such as that in 1999, represent a strategy may reduce local risks. (k) Spatial harvest inequity (measured as the absolute mean relative error from perfect equity). Note that in 1999 equity differs depending on which benchmark is used (IFD or uniform proportional harvest).

Spatial allocation of harvest

The fishing fleet either distributes itself in space or a manager forces spatial allocation. We use three scenarios for spatial allocation: 1) diffuse effort in space (i.e harvest is proportional to abundance), 2) ideal distribution of effort in space, and 3) random spatial allocation.

Proportional allocation of harvest

For a proportional allocation of harvest, the calculation of biomass caught in each location ($\mathrm{H}_{l,t}$) is simply:

$$H_{\mathrm{adults}_{l,t}} = \frac{\sum_{a=2}^{10} \mathrm{w}_a \mathrm{m}_a n_{a,l,t}}{\sum_{l=1}^{L} \sum_{a=2}^{10} \mathrm{w}_a \mathrm{m}_a n_{a,l,t}} \times \mathrm{Quota}_t \tag{S.10}$$

Ideal free distribution

For the Ideal Free Distribution of Effort in Space, the fishing fleet would ideally allocate themselves to optimize efficiency of catch (i.e. minimal effort for the return). We can numerically solve for the spatial harvest strategy that optimizes efficiency using a system of ordinary differential equations (ODEs). First, we 1) simplify the fishery to a very short time period, 2) assume vessels can move instantaneously among locations with no cost, 3) assume vessels have perfect information and 4) assume fishing effort (i.e. sets) can be broken into infinitesimally small units. Consider $F_{l,\tau}$ the rate of fishing effort (i.e. number of sets per unit time) allocated at time τ in location l, q is the catchability of fish (i.e. ratio of proportional capture rate to effort), B_τ is the biomass available for capture at time τ D_e is the rate at which vessels respond to spatial disparities in efficiency, where efficiency = effort x catchability x biomass. To maximize efficiency, vessels sense disparities in efficiency and move instantaneously to neighboring locations with higher efficiency (i.e. catch per unit time per unit effort).

$$\frac{dB_l}{d\tau} = -F_l(\tau) q B_l(\tau) \tag{S.11a}$$

$$\frac{dF_l}{d\tau} = \sum_{j=1}^{L} \left[F_l(\tau) q B_l(\tau) - F_j(\tau) q B_j(\tau) \right] \tag{S.11b}$$

$$\frac{dH_l}{d\tau} = F_l(\tau) q B_l(\tau) \tag{S.11c}$$

$$\mathrm{H}(\tau_Q, l) = \int_0^{\tau_Q} F_l(\tau) q B_l(\tau) d\tau \tag{S.12a}$$

$$\mathrm{StockH}(\tau_Q) = \sum_{l=1}^{L} \mathrm{H}(\tau_Q, l) \tag{S.12b}$$

We numerically evaluate this system of ODEs until the quota is achieved to produce the final, optimal distribution of catch in space.

Random spatial allocation distribution

For random distribution of the harvest, the proportion of the quota removed from each location within each year is a random draw from a Dirichlet distribution, with mean equal to the actual proportional biomass distribution.

random proportional harvest rates are assigned to each site, with a maximum proportion of biomass removed at any given spawning site.the fleet randomly chooses a site, prosecutes a fishery, and moves on until the quota is achieved. Functionally, the fleet effort is distributed randomly in space, with mean allocation probabilities given by the distribution of biomass in space. Potential, proportional harvest rates are randomly assigned to each spawning area (though cannot exceed the maximum) and prosecuted in order from highest to lowest until the quota is achieved. The initial random proportional harvest rates are set by a Dirichlet distribution where means are proportional to the distribution of stock biomass in space and a count parameter (K) that sets the degree of randomness (set as $K = 5$) to achieve a spatial harvest inequity of approximately 0.20. Lower count parameters defy the proportionality more (i.e. harvests are unlikley to reflect biomass distributions in space) while very high count parameters approximate harvests that are porportional to biomass distributions in space. An example of random harvest allocation is given by Figure S.3.

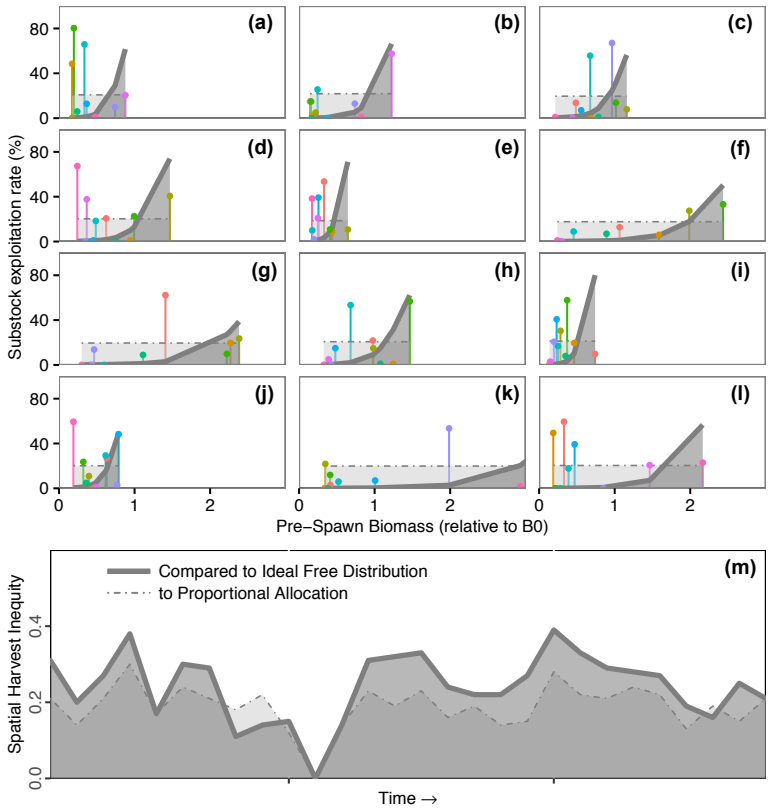

Figure S.3: Examples of implementation of random harvest allocation for individual years in the simulation model for a target harvest of 20%. Each panel represents one year with 10 substocks. Vertical bars with points represent substock harvest rates compared to the relative pre-spawn (and pre-harvest) biomass in that substock.

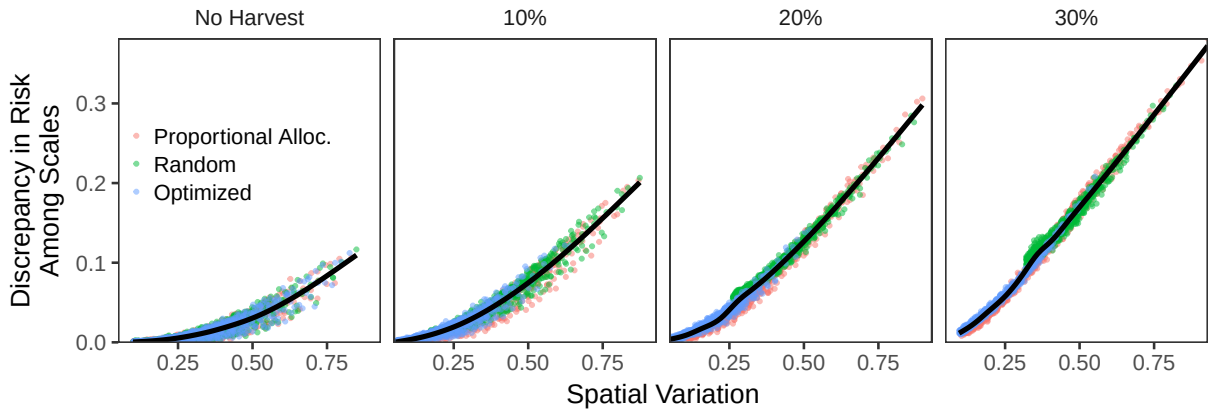

Figure S.4: Discrepancy in risk among spatial scales (mean risk at subpopulation scale minus mean risk at metapopulation scale) versus spatial a variance by harvest rate and spatial harvest allocation strategy

.

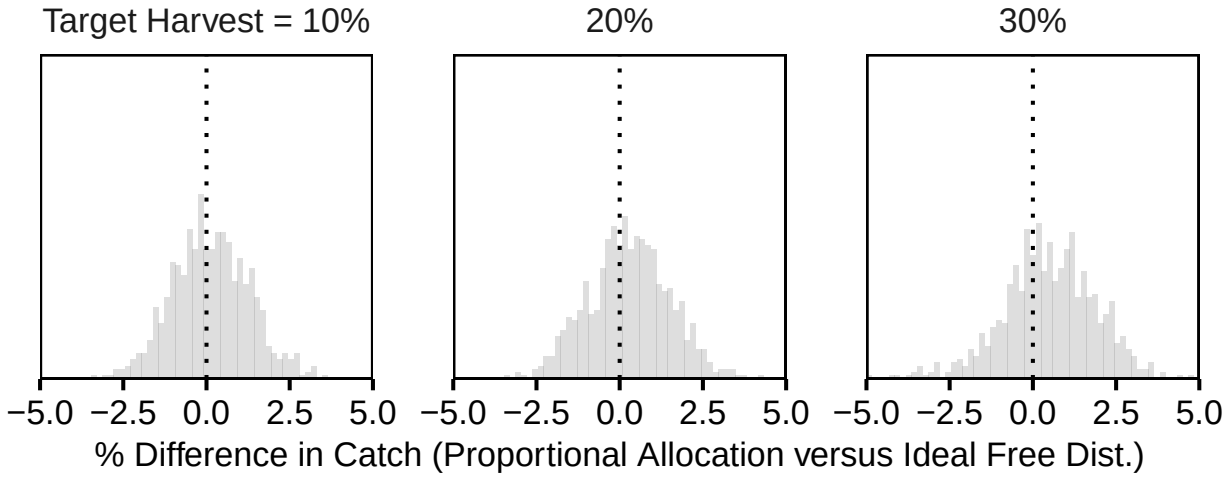

Figure S.5: Relative frequency of the % difference in catch between proportional allocation and ideal free distribution of harvest, calculated for each individual simulation scenario as $100 * \left(\overline{catch}_{PA} - \overline{catch}_{IDF}\right) / \overline{catch}_{PA}$

.

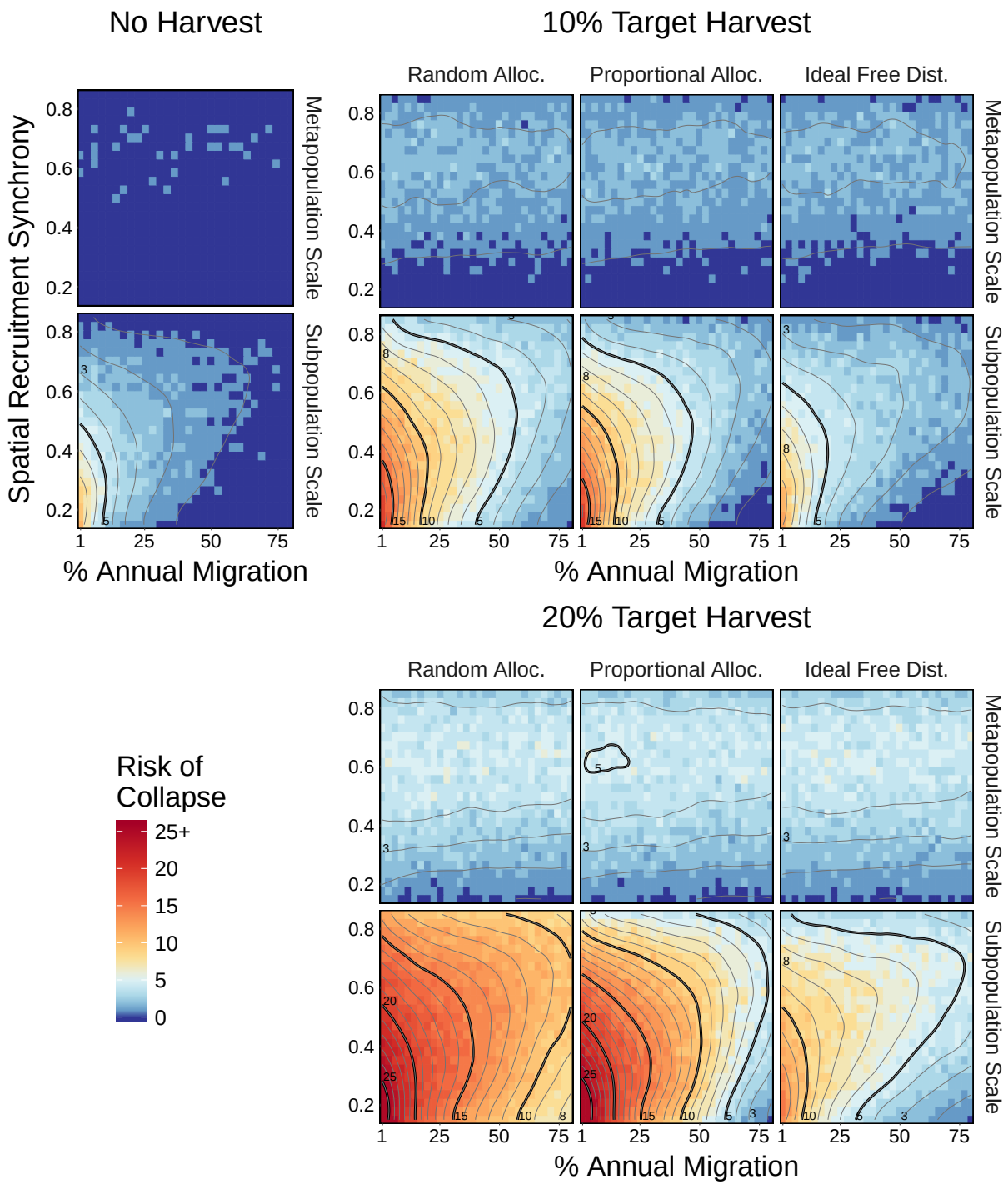

Figure S.6: Simulation results including target harvest rates ranging from 0 to 20% for each spatial allocation scenario and measured at the metapopulation (stock) and population (substock) scales. 30% harvest rate not shown due to all risk panels above 10%

Statistical properties of the VAR(1) model

The long-term temporal variability of the individual populations and the metapopulation is determined by the long-run covariance matrix:

$$\mathrm{vec}(\boldsymbol{\Sigma}_x) = \left[\boldsymbol{I}_{p^2} - \boldsymbol{J} \otimes \boldsymbol{J}\right]^{-1} \mathrm{vec}(\boldsymbol{\Sigma}_\zeta) \tag{S.13}$$

Where p is the total number of variables (i.e. reproducers, recruits, and adult stages in both populations), $\boldsymbol{I}_{p^2}$ is a $p^2 \times p^2$ identity matrix, $\otimes$ is the Kronecker product, and vec is the vector operator (i.e. turning a matrix into a vector for operational sake). The population and metapopulation coefficient of variation (on the natural scale), as well as the among population spatial variation and spatial correlations the can be derived from $\boldsymbol{\Sigma}_x$ using the definition of the mean, variance and covariance of a multivariate lognormal given the mean and covariance matrix of the log-scale system (see appendix for derivations).

If we assume the system conforms to a multivariate lognormal, the temporal variance of spawners at site i is:

$$\mathrm{Var}(e^{[x_{i,a_0}]}) = e^{[2\bar{x}_{i,a_0} + \sigma^2_{i,i}]} e^{[\sigma^2_{i,i} - 1]} = e^{[\sigma^2_{i,i}]} e^{[\sigma^2_{i,i} - 1]} \tag{S.14}$$

where $\sigma^2_{i,i}$ is the diagonal element of the log-scale variance covariance matrix $\boldsymbol{\Sigma}_x$ associated with spawners at site i (x_{i,a_0}), and $\bar{x}_{i,a_0}$ is the mean of x_{i,a_0} which is set to zero. From the lognormal, the mean of $e^{[x_{i,a_0}]}$ is $e^{[0.5\sigma^2_{i,i}]}$.

The resulting coefficient of variation of each spawning population is:

$$\mathrm{CV}(e^{[x_{i,a_0}]}) = \frac{\sqrt{e^{\left[\sigma^2_{i,i}\right]} e^{\left[\sigma^2_{i,i} - 1\right]}}}{e^{\left[0.5\sigma^2_{i,i}\right]}} = \sqrt{e^{\left[\sigma^2_{i,i} - 1\right]}} \tag{S.15}$$

The temporal covariance of scaled spawners among sites is:

$$\mathrm{Cov}(e^{[x_{i,a_0}]}, e^{[x_{j,a_0}]}) = e^{[0.5\sigma^2_{i,i} + 0.5\sigma^2_{j,j}]} e^{[\sigma^2_{i,j} - 1]} \tag{S.16}$$

where $\sigma^2_{i,j}$ is the off-diagonal (covariance) element of $\boldsymbol{\Sigma}_x$.

Considering a metapopulation with two component populations, we set the log-population variances equal (i.e. $\sigma_{i,i} = \sigma_{j,j} = \sigma$), the resulting variance of the spatial mean on the natural scale is:

$$\mathrm{Var}\left[\frac{e^{[x_{i,a_0}]} + e^{[x_{j,a_0}]}}{2}\right] = \mathrm{Var}\left(\frac{e^{[x_{i,a_0}]}}{2}\right) + \mathrm{Var}\left(\frac{e^{[x_{j,a_0}]}}{2}\right) + 2\mathrm{Cov}\left(\frac{e^{[x_{i,a_0}]}}{2}, \frac{e^{[x_{j,a_0}]}}{2}\right) \tag{S.17}$$

$$= 0.5e^{[\sigma^2]} e^{[\sigma^2 - 1]} + 0.5e^{[\sigma^2]} e^{[\sigma^2_{i,j} - 1]} \tag{S.18}$$

Thus, the temporal coefficient of variation of the spatial mean is:

$$\mathrm{CV}\left[\frac{e^{[x_{i,a_0}]} + e^{[x_{j,a_0}]}}{2}\right] = \frac{\sqrt{0.5e^{[\sigma^2]} e^{[\sigma^2 - 1]} + 0.5e^{[\sigma^2]} e^{[\sigma^2_{i,j} - 1]}}}{e^{[0.5\sigma^2]}} = \sqrt{0.5e^{[\sigma^2 - 1]} + 0.5e^{[\sigma^2_{i,j} - 1]}} \tag{S.19}$$

In this case, the residual spatial variance (taken from S.7) is:

$$\text{residual spatial variance} = 0.5e^{[\sigma^2]}e^{[\sigma^2-1]} - 0.5e^{[\sigma^2]}e^{[\sigma^2_{i,j}-1]} \tag{S.20}$$

Which when standardized by the square of the population mean ($e^{[0.5\sigma^2]}$) yields:

$$\text{standardized residual spatial variance} = 0.5e^{[\sigma^2-1]} - 0.5e^{[\sigma^2_{i,j}-1]} \tag{S.21}$$

In this case this is the same as the variance of the difference between either population and the population mean trend (because both populations are identical).

$$\begin{aligned}
\mathrm{Var}\left[e^{[x_{i,a_0}]} - \left(\frac{e^{[x_{i,a_0}]} + e^{[x_{j,a_0}]}}{2}\right)\right] &= \mathrm{Var}\left[\frac{e^{[x_{i,a_0}]}}{2} - \frac{e^{[x_{j,a_0}]}}{2}\right] && \text{(S.22)}\\
&= \mathrm{Var}\left[\frac{e^{[x_{i,a_0}]}}{2}\right] + \mathrm{Var}\left[\frac{e^{[x_{j,a_0}]}}{2}\right] - 2\mathrm{Cov}\left(\frac{e^{[x_{i,a_0}]}}{2}, \frac{e^{[x_{j,a_0}]}}{2}\right) && \text{(S.23)}\\
&= 0.5e^{[\sigma^2]}e^{[\sigma^2-1]} - 0.5e^{[\sigma^2]}e^{[\sigma^2_{i,j}-1]} && \text{(S.24)}
\end{aligned}$$

As a result, we can combine the solutions from C.13 and C.21 to generate the residual spatial variation for the metapopulation and how it is influenced by mortality and environmental correlations.

Autocorrelations

The matrix of first-order autocorrelations that yields within population correlation and spatial coupling is given by:

$$\mathbf{R} = (\mathrm{diag}(\mathbf{\Sigma}_x)^{\circ\frac{1}{2}})^{-1}\mathbf{\Sigma}_x(\mathrm{diag}(\mathbf{\Sigma}_x)^{\circ\frac{1}{2}})^{-1} \tag{S.25}$$

Impulse response of the VAR(1) model

The impulse response (IR) of adults at location i after a lag t to a single pulse log-scale recruitment deviation is the first coefficient of the nth column of the moving average (MA) representation of the VAR model. Specifically, the matrix of MA coefficients for the VAR(1) at lag t is produced by $\mathbf{J}^t$. In this case, the IR for adults is the first entry of the corresponding MA vector. The greatest IR of adults is at lag 1 (when a recruitment pulse first enters into the adult stage) and is thus conveniently represented by the first entry of the jacobian matrix $\mathbf{J}$. Because this represents the log-scale additive response, the IR on the natural scale is a multiplicative effect.